MODELS FOR ESTIMATION OF ISOMETRIC WRIST JOINT TORQUES USING SURFACE ELECTROMYOGRAPHY

by

Amirreza Ziai
B.Eng., Sharif University of Technology, Tehran, 2008

THESIS SUBMITTED IN PARTIAL FULFILLMENT OF
THE REQUIREMENTS FOR THE DEGREE OF

MASTER OF APPLIED SCIENCE

In the
School of Engineering Science
Faculty of Applied Science

SIMON FRASER UNIVERSITY

Fall 2011

APPROVAL

Name: **Amirreza Ziai**

Degree: **M.A.Sc**

Title of Thesis: **Models for estimation of isometric wrist joint torques using surface electromyography**

Examining Committee:

Chair: **Parvaneh Saeedi, P.Eng**
Assistant Professor – School of Engineering Science

_____

Dr. Carlo Menon, P.Eng
Senior Supervisor
Assistant Professor – School of Engineering Science

_____

Dr. Shahram Payandeh, P.Eng
Supervisor
Professor – School of Engineering Science

_____

Dr. Bozena Kaminska, P.Eng
Examiner
Professor – School of Engineering Science

Date Defended/Approved: _____September 2, 2011 _____

Declaration of
Partial Copyright Licence

SFU SIMON FRASER UNIVERSITY
THINKING OF THE WORLD

STATEMENT OF ETHICS APPROVAL

The author, whose name appears on the title page of this work, has obtained, for the research described in this work, either:

(a) Human research ethics approval from the Simon Fraser University Office of Research Ethics,

or

(b) Advance approval of the animal care protocol from the University Animal Care Committee of Simon Fraser University;

or has conducted the research

(c) as a co-investigator, collaborator or research assistant in a research project approved in advance,

or

(d) as a member of a course approved in advance for minimal risk human research, by the Office of Research Ethics.

A copy of the approval letter has been filed at the Theses Office of the University Library at the time of submission of this thesis or project.

The original application for approval and letter of approval are filed with the relevant offices. Inquiries may be directed to those authorities.

Simon Fraser University Library
Simon Fraser University
Burnaby, BC, Canada

Last update: Spring 2010

ABSTRACT

With an aging population, facilitation of an independent lifestyle for the elderly and those with neuromuscular conditions is a prominent field of research. Different robotic prototypes have been proposed in order to aid patients and seniors regain their autonomy by augmenting forces exerted by the device wearer. Some of these prototypes are controlled in force by processing surface electromyography (SEMG) signals acquired from wearer's muscles. However, the accuracy of the estimated force may deteriorate with passage of time and alteration of limb configurations. SEMG and isometric torque data are recorded from eleven healthy volunteers to (1) compare the accuracy of six torque estimation models and (2) demonstrate estimation accuracy preservation under arm varying configurations. The research focuses on wrist extension/flexion in order to simplify the performed analysis.

Keywords: surface electromyography (EMG); joint torque estimation; joint torque estimation models.

Dedicated to Roya,

Mahmoud and Niloufar

ACKNOWLEDGEMENTS

I would like to thank my senior supervisor, Dr. Carlo Menon, without whom this work would have never reached fruition. I would also like to thank all the members of the examining committee for their priceless suggestions.

My sincere gratitude goes to my family for their unconditional love and support throughout my life. I am grateful to their selfless blessing and support.

I would like to thank Dr. Shahram Payandeh, Dr. Maxwell Donelan, Dr. Gary Wang, and Dr. Ryozo Nagamune for providing me with their invaluable insight throughout this journey.

I would like to thank all current and previous members of the MENRVA lab, in particular Bastian Tietjen, Cormac Sheridan, Farzad Khosrow-khawar, Gil Herrnstadt, Michael Henrey, Mojgan Tavakolan, Zeeshan Khokhar, and Zhen Gang Xiao.

TABLE OF CONTENTS

LIST OF FIGURES

LIST OF TABLES

CHAPTER 1 INTRODUCTION

1.1 Motivation

A fully functioning upper limb is crucial for autonomy of individuals. However, aging, disease, and neuromuscular conditions can impair the functionality of the upper limb. In Canada, 300,000 people are living with a disability [1].

Rehabilitation is an effective method for restoring motor abilities of individuals with impaired functionality. Intense and task-oriented rehabilitation promote motor recovery and cerebral reorganization [2]. Therapists initially examine patients for presence of pain, loss of strength, sensation, and range of motion. They evaluate functional performance mainly by subjective observations and utilization of standardized tests. Unfortunately, consistency of assessments is lost when more than one therapist works with the same patient and objective assessment of patient progress is rendered impractical. Furthermore, long rehabilitation sessions generally required for extended periods is an enormous economic burden; requiring highly trained professionals and equipped facilities.

With an aging population and an increased demand for rehabilitation, robotic devices have been considered as a supplemental therapy method. These devices can move patient's limbs repetitively in a pre-specified range of motion for long sessions. Moreover, robots equipped with sensors, can provide the therapist with more accurate and objective evaluation of patient's progress.

Rehabilitative robots are operated in two modes: rehabilitation and assistance. In the rehabilitation mode, patients do not attempt to move his or her limb while the robot does all the work. In the assistance mode, the robot supplements movement efforts.

Surface electromyography (SEMG) signals can be used to estimate the direction and magnitude of torques about a joint. SEMG signals, picked up non-invasively from the surface of the skin, are a measure of muscle activity. Increased level of muscle activity is an indication of higher forces produced by muscles and higher joint torques consequently. Assistive robotic devices utilize these signals as control inputs.

Researchers have developed several regression and classification methods for estimation of joint torques based on SEMG signals. We first provide a quantitative comparison of the most commonly used methods using experimental SEMG and torque signals gathered from eleven healthy volunteers. Subsequently, we propose and demonstrate the viability of a joint torque estimation model that is insensitive to varying arm configurations. We showed that testing accuracy increases with training models with data gathered from different arm configurations. Moreover, we demonstrated that the model training time does not noticeably increase with addition of training data, making the model more desirable for training at numerous configurations.

1.2 Objectives

Objectives of this thesis are as follows:

a) Devise a protocol for gathering experimental SEMG and torque data, which captures the phenomena that result in accuracy deterioration of joint torque estimation models.

b) Quantify the effects of number of muscles, arm configuration alterations, passage of time, and electrode displacement on accuracy of joint torque estimation models.

c) Identify the most suitable model that addresses accuracy deterioration of wrist torque estimation due to alteration of arm configurations.

d) Demonstrate the viability of the proposed model for estimation of isometric wrist joint torques under varying arm configurations.

1.3 Thesis Structure

This chapter discussed the motivation and objectives of this work. The remaining chapters are structured as follows:

Chapter 2 discusses the importance of upper limb for autonomy of individuals. Common causes of upper limb function impairment are discussed and rehabilitation methods are overviewed. Robotic devices are subsequently presented as a viable therapy method. Technologies used in these devices and design trade-offs are discussed. Finally, SEMG signals are introduced and torque estimation models based on these signals are discussed.

Chapter 3 describes the estimation models used for estimation of isometric joint torques in this study.

Chapter 4 describes the experimental setup and protocol used for gathering experimental data used for quantifying the performance of models.

Chapter 5 quantifies and compares the performance of different joint torque estimation models.

Chapter 6 proposes a modified linear regression model that is demonstrated to be a remedy to deterioration of model accuracy with varying joint angles and alteration of limb configurations.

Chapter 7 concludes the thesis and discusses potential future work.

CHAPTER 2 BACKGROUND

2.1 Upper Limb

Human upper limb is very important for performing cognitive-driven and expression-driven tasks, as well as exploration and manipulation of the surrounding space. The high degree of mobility of the kinematic chain composed of shoulder, arm, elbow, wrist, and hand, allows positioning the hand for various functional activities.

A hand with full functionality is essential for independent and active lifestyle. Unfortunately, due to the complex structure of the upper limb and its central role in interaction with the environment, it is highly prone to injuries. Neuromuscular diseases and stroke also frequently impair the functionality of the upper limb [3]. Almost 450,000 Americans suffer from multiple sclerosis and muscular dystrophy that result in loss of hand strength and dexterity [4]. In Canada, more than 50,000 individuals have multiple sclerosis [5]. Approximately 40% of emergency treatment of surgery and orthopaedics is associated to hand trauma [6]. Arm function is also acutely impaired in the majority of stroke survivors [7].

Loss of muscle mass due to aging, known as sarcopenia or frailty is another contributor to decreased level of functionality [8]. Prevalence of sarcopenia is believed to be about 30% of the population of people 60 years and older [9].

2.2 Wrist

Important activities of daily living such as eating with a spoon, writing and painting, drinking from a cup, and using a wheelchair are dependent on functionality of the wrist. Wrist joint connects the hand and forearm. This joint possesses two degrees of freedom: flexion-extension and ulnar-radial deviation. Flexion is bending of the wrist so the palm approaches anterior surface of the forearm, whereas extension is the motion in the reverse direction. Radial deviation, also known as abduction, is bending the wrist to the thumb side, whereas ulnar deviation is the bending of the wrist towards the little finger [10]. Figure 2-1 demonstrates wrist flexion/extension and radial/ulnar deviation.

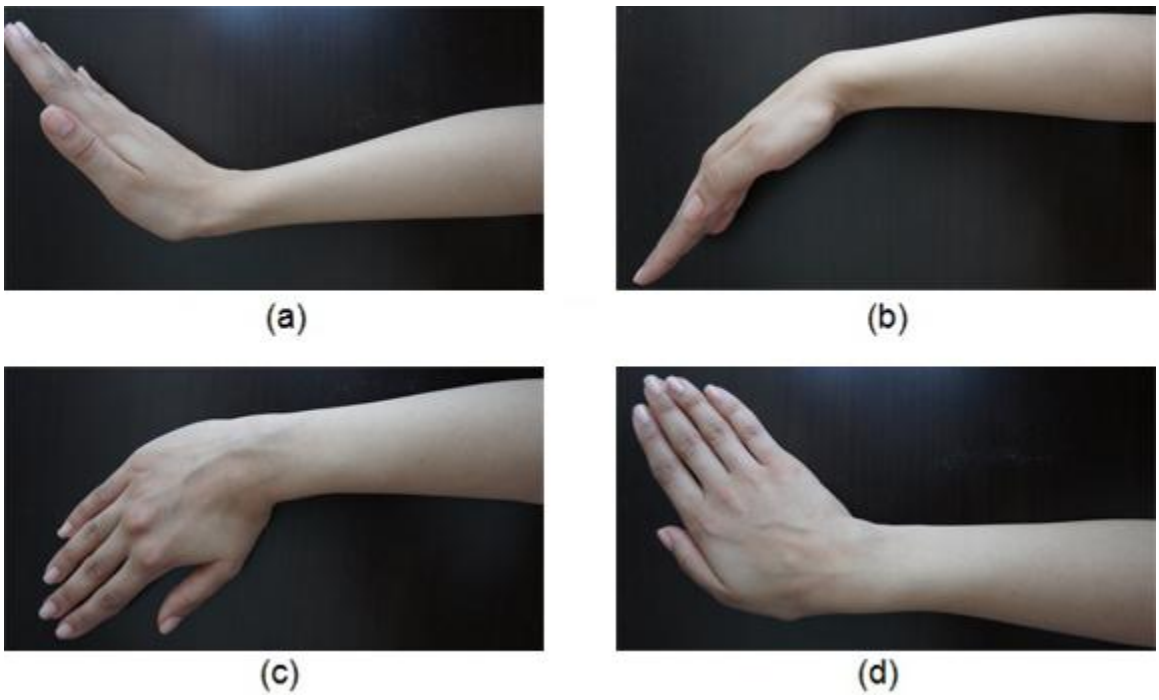

Figure 2-1: Wrist joint degrees of freedom.
(a) Wrist extension, (b) wrist flexion, (c) radial deviation, (d) ulnar deviation

Activities of daily living (ADL) such as opening a jar, turning a doorknob, and pushing up from a chair are severely restricted following impairment of the wrist [11]. Brain map research suggests that motor cortical representation expand with activity following stroke and traumatic injury [12]. Therefore, long rehabilitation training sessions focused on intensive task-oriented repetitive movements is beneficial to the recovery of wrist functionality [13]. Tasks that focus on ADL have shown significant increase in motor recover post stroke [14]. However, rehabilitation in presence of therapists, who are in relative shortage, is resource and cost intensive [15].

Robotic devices are nowadays a viable supplement to therapy. Robots can facilitate repetitive movement of impaired limbs without fatigue, provide accurate progress measurements, and can be independently used by patients living in remote areas without daily access to therapists.

2.3 Rehabilitative and Assistive Devices

Exoskeletons are a set of mechanical linkages that are attached to the body. In a mechatronics context, exoskeletons are devices worn by a person that permit direct transfer of mechanical power and exchange of information through actuators and sensors. A group of researchers at Cornell University and General Electric developed the first master-slave exoskeleton in early 1970s [16]. Initially, most exoskeletons were designed for teleoperation and power amplification. An example is the exoskeleton shown in Figure 2-2 that fits over the gloved hand of an astronaut and enables amplification of astronaut’s power [17].

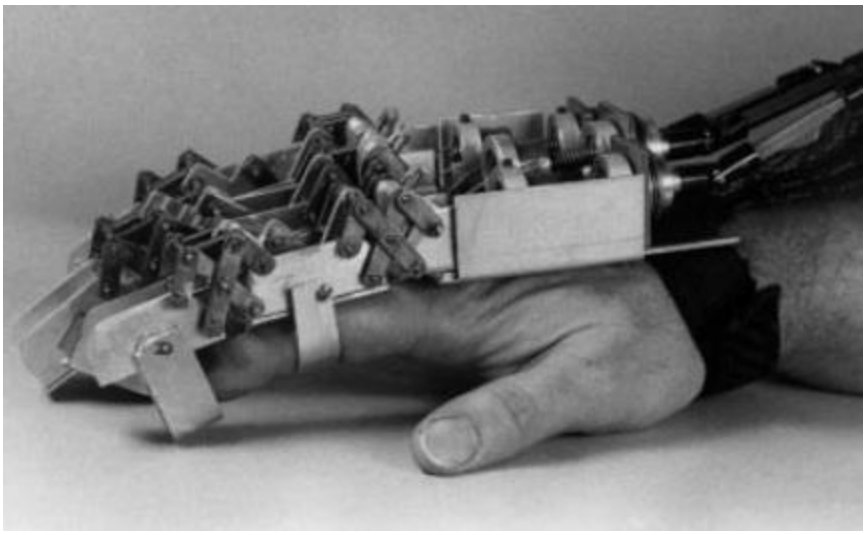

Figure 2-2: Power augmentation exoskeleton. Reproduced from [17].

Three actuated fingers, controlled by pressure signal input from pressure sensors mounted between exoskeleton and the hand help the astronaut in overcoming the suit stiffness and performing tasks that would normally fatigue their hands. Considering only three fingers, combining the middle and ring fingers reduced the overall size and complexity of the mechanism.

Teleoperation robots are exoskeletons that enable force-feedback telemanipulation using a master-slave system. Telepresence makes execution of tasks dependent on human judgment possible in harsh and dangerous environments such as outer space or nuclear plants [18]. Figure 2-3 shows an example of a human arm exoskeleton that allows immersion of the operator in the working space using force feedback.

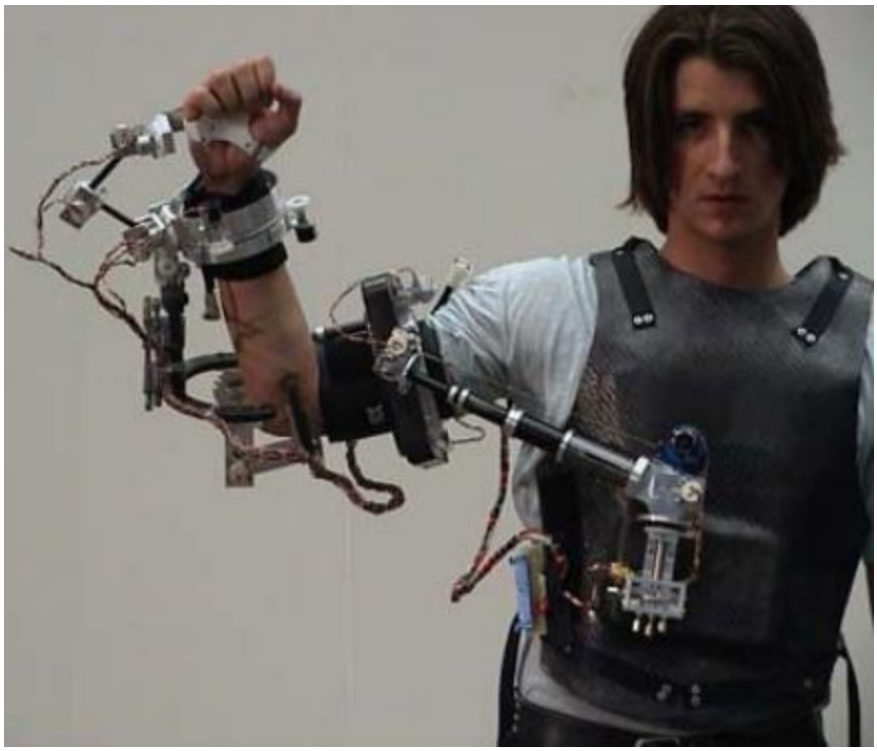

Figure 2-3: Teleoperation exoskeleton. Reproduced from [18].

The ESA arm exoskeleton is wearable and motors sitting on the chest-plate drive joints through cables. The exoskeleton is designed in such a way that the thorax and not the arm carry its weight. Arm movements are measured using sensors and the robotic arm replicates them in real-time. Force sensors on the robotic arm measure interaction forces. For instance, when the robotic arm hits an obstacle along its way, force sensors measure these forces. Exoskeleton's controller then generates signals that would apply the same amount of force to appropriate joint using the actuator system. Figure 2-4 depicts the interactions between the exoskeleton and the robotic arm.

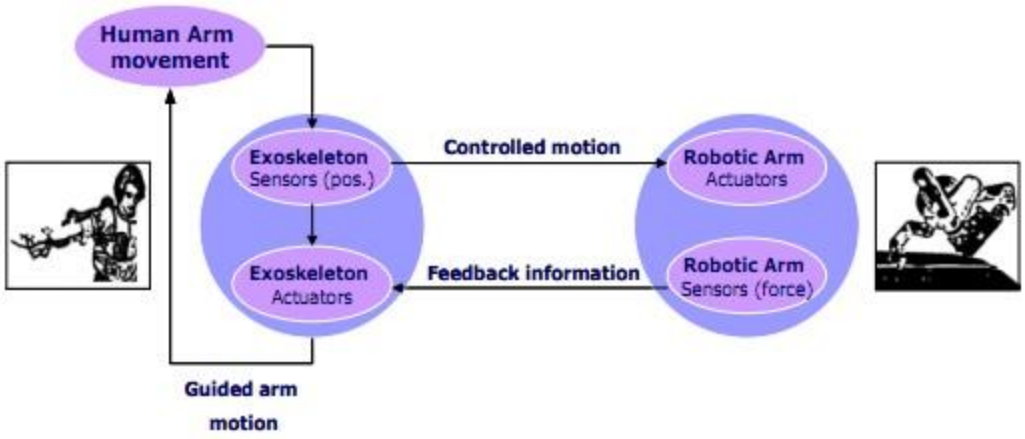

Figure 2-4: Interaction between exoskeleton and robotic arm. Reproduced from [18].

More recently, researchers have designed exoskeletons for rehabilitation and assistance of stroke patients and the elderly. Unfortunately, there exist numerous challenges and trade-offs to the design of such systems. Rigid parts that transmit forces to the human body, actuators that drive these linkages, electronics and power sources have substantial weight. The first challenge is to design exoskeletons in such a way that the impaired limb carries the least possible weight. Second, presence of bulky linkages and actuators sometimes limits the affected limb's motion. Specially, the palm area should be free of mechanical elements so that the user's interaction with his or her surroundings is not hindered. Moreover, the device should be backdrivable, meaning that the exoskeleton should be transparent to the user so he can freely move his limb around. Friction between moving parts of linkages, gears, and non-backdrivable actuators limit backdrivability of exoskeletons.

Rehabilitation devices generally do not require intelligent control inputs. Therapists program such devices so that patient can receive suitable therapy. For example, stroke patients with no functional movement mainly need passive movements [19]. In other rehabilitation methods, such as mirror therapy, movement of the unaffected limb generate the signals required for controlling the affected one [20]. Figure 2-5 shows how the affected hand is controlled using the data received from a set of sensors embedded in a data glove.

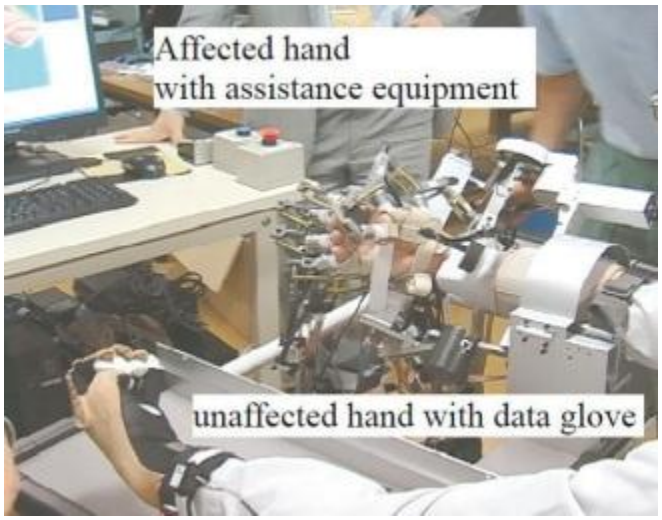

Figure 2-5: Mirror therapy using robotics. Reproduced from [20].

Assistive devices, on the other hand, allow for amplification of the forces generated by the user. Researchers and engineers have designed numerous rehabilitative and assistive devices, some of which are commercially available. We will present a few of these devices to demonstrate the latest available technologies and challenges currently faced by designers of rehabilitative and assistive devices.

The first example is a wearable device controlled by two pneumatic muscles [21]. Figure 2-6 shows the exoskeleton while providing assistive forces for finger and thumb extension.

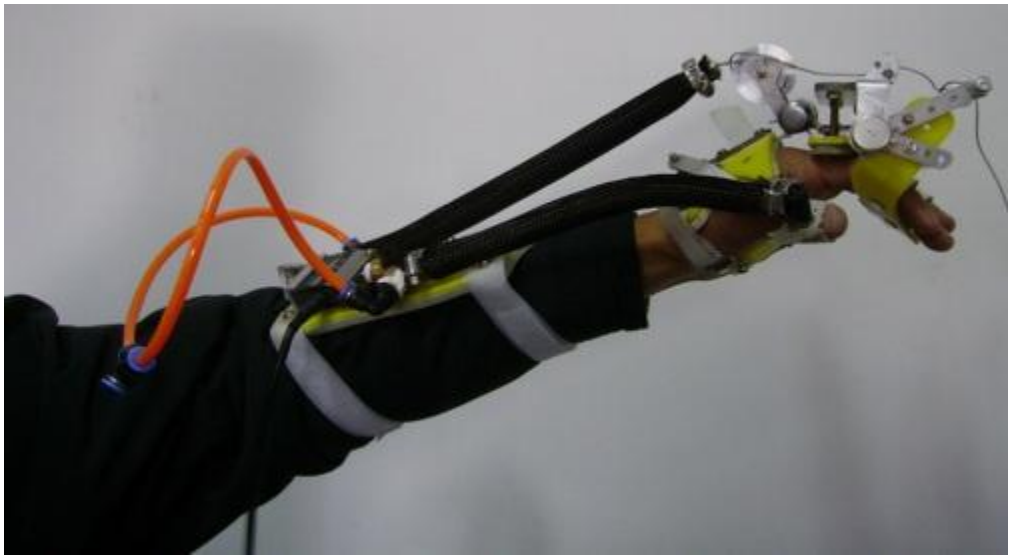

Figure 2-6: Pneumatic assistive device. Reproduced from [21].

Each pneumatic actuator can pull the cable connected to each that in turn moves the linkages connected to it. This setup allows extension of the fingers and the thumb independently. Stroke patients frequently exhibit spasticity that is an increase in muscle tone and reduced ability to stretch muscles [22]. Therefore, extending fingers for stroke patients poses a bigger challenge than flexing them and this device targets only finger extension. Pneumatic actuators used in this design are lightweight and inexpensive; however, these actuators exhibit non-linear behaviour that makes their control challenging.

Second example is an exoskeleton with three active degrees of freedom for the index finger, three active joints for the combination of the middle, ring and little fingers as well as two active degrees of freedom for the thumb [23]. A five-link mechanism also assists the user's wrist movements. Figure 2-7 shows the exoskeleton.

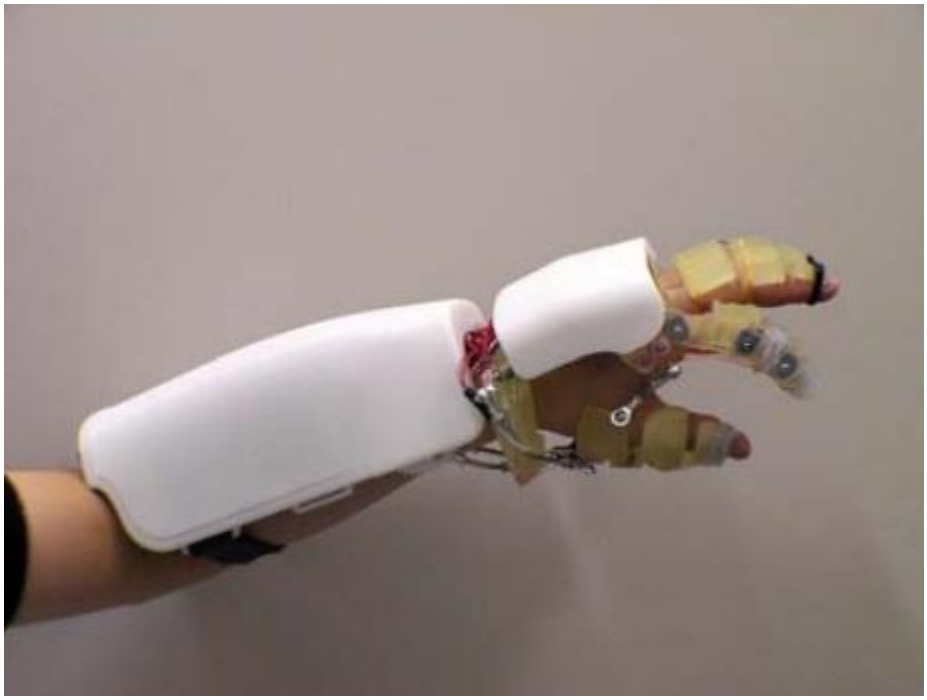

Figure 2-7: Assistive device for wrist and fingers. Reproduced from [23].

The tendon drive mechanism utilized in this design allows for stable grasping as it increases the mechanical compliance of the fingertips. This backdrivable mechanism assists the wearer only when he needs a large grasping force and is transparent to the user in other times.

Hand Wrist Assistive Rehabilitative Device (HWARD) is a device intended to assist patients with power grip [24]. Pneumatic cylinders flex and extend the wrist, four fingers and the thumb. Movement is only supported at the most proximal finger and thumb joints (MCP). Pneumatic cylinders can generate adequate forces for rehabilitating the wrist. Figure 2-8 shows a patient using HWARD.

Figure 2-8: Grip assistance device. Reproduced form [24].

HWARD is equipped with redundant safety measures that prohibit overexertion of patient's muscles. However, HWARD confines the patient to a stationary setting, as the equipment supporting actuation is not portable.

Researchers have designed a portable device, capable of extending the wrist developed in the MENRVA lab at Simon Fraser University [25]. Extension of

the wrist is particularly important for stroke survivors who generally lack that ability. This simple design utilizes a linear actuator that pulls on a string connected to the wearer's palm via a cantilever structure, resulting in extension of the wrist. Figure 2-9 shows the device.

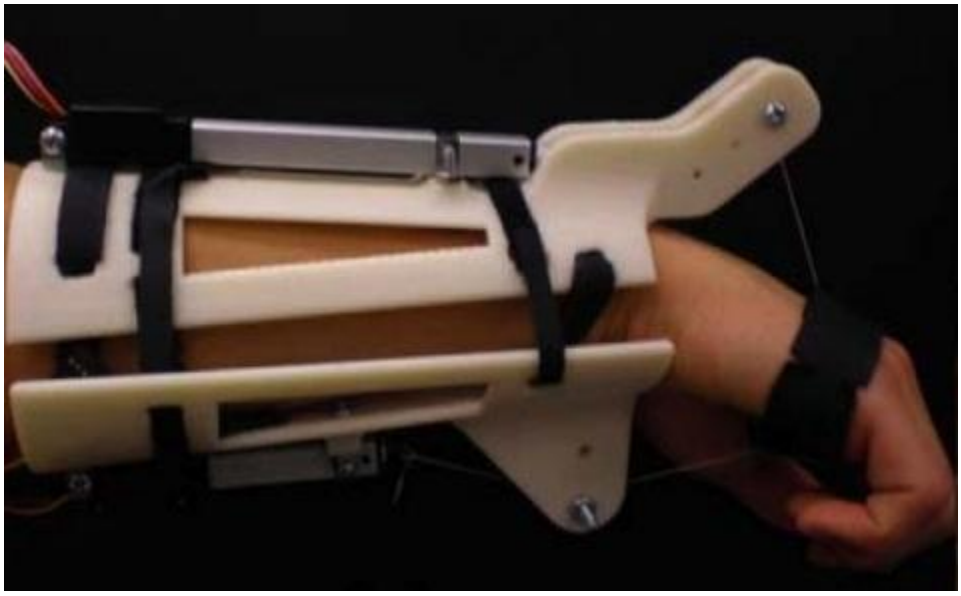

Figure 2-9: Wrist rehabilitation device for stroke patients. Reproduced from [25].

The device can produce more than 50% of the maximum average isometric joint torque generated by test subjects in the study conducted [25]. Compact and lightweight design of the system, and low voltage requirements of the linear actuator, make it ideal for portable applications. However, as the patient flexes or extends his hand away from the neutral position, less torque is applied about the wrist joint by the same amount of actuator force because of the mechanical design of the system.

Wrist Exoskeleton Prototype (WEP) is another example of a portable and lightweight (about 500g) device providing assistive and rehabilitative forces to the wrist [26]. WEP supports two actuated degrees of freedom: wrist flexion/extension and ulnar/radial deviation. WEP is shown in Figure 2-10.

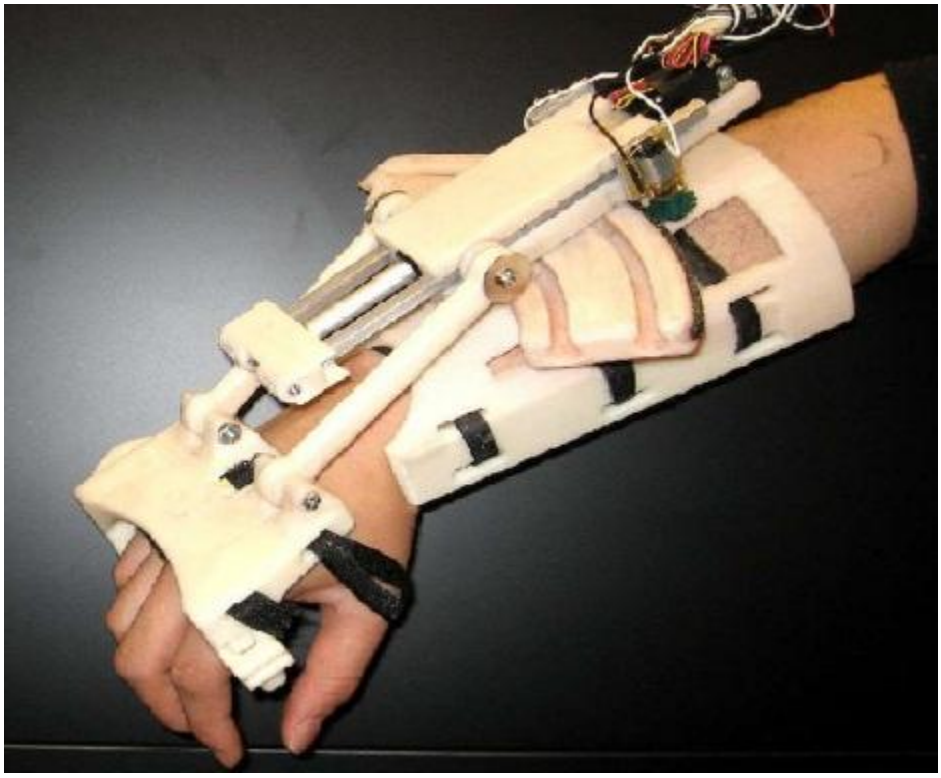

Figure 2-10: Wrist Exoskeleton Prototype (WEP). Reproduced from [26].

A linear actuator flexes and extends the wrist with 2.2 Nm of torque, whereas a gear motor actuates the ulnar/radial degree of freedom. The actuated ulnar/radial degree of freedom can apply a maximum torque of 5.4 Nm. Motors are controlled independently of each other using biological signals acquired from the patient's forearm. Experiments conducted demonstrated that the WEP

controller can estimate the direction and magnitude of torques applied by the user with an average accuracy of 96%. However, only isometric wrist motions at the neutral wrist position (position that the wrist assumed when at rest, with a straight and unbroken wrist) have been considered in the design of the controller. It should be noted that isometric contraction of a muscle implies activation of muscle without a change in muscle length. An example of this type of contraction is when a person holds a weight in front of them. In this case, muscles are activated as they are opposing the gravitational force, even though the weight is not moving. Other types of contraction involve changes in muscle length.

Joystick and voice commands have been used for controlling assistive devices. However, SEMG signals acquired using surface electrodes, allow for seamless integration with the body and intuitive control of assistive devices [27].

2.4 Surface Electromyography

SEMG is a well-established technique for non-invasive recording of electrical activity produced by muscles. Signals recorded at the surface of the skin are picked up from all the active motor units near the electrode [28]. Motor units are motor neurons that contract all fibres that they control when activated. Each muscle is controlled by a combination of motor units. Due to the convenience of signal acquisition from the surface of the skin, SEMG signals have been used for controlling prosthetics and assistive devices [29-33], speech recognition systems [34], and also as a diagnostic tool for neuromuscular diseases [35].

However, analysis of SEMG signals is complicated due to several factors. First, cross talk between the adjacent muscles complicates recording signals from a muscle in isolation [37]. Second, signal behaviour is very sensitive to the position of electrodes [38]. Moreover, even with a fixed electrode position, altering limb positions have been shown to have substantial impact on SEMG signals [39]. Other issues, such as inherent noise in signal acquisition equipment, ambient noise, skin temperature, and motion artefact can potentially deteriorate signal quality [40, 41]. More information about SEMG signal characteristics is available in Appendix A.

2.5 Force/torque estimation using SEMG

Amplitude of SEMG signals acquired from a muscle is correlated with the forces produced by that muscle. This correlation, however, is not a linear one. Classification [42] and regression models [43, 44], as well as physiological models [45, 46], have been considered for mapping this relationship. Machine learning classification in aggregate has proven to be viable methods for classifying limb configurations [47] and joint torque levels [48]. Park et al. [49] compared the performance of a physiological model, linear regression and artificial neural networks for estimation of thumb-tip forces under four different configurations. In another study, performance of a physiological model was compared to a neural network for estimation of forearm flexion and extension joint torques [50]. Both groups showed that neural network predictions are superior to physiological models, but neural network estimations are task specific and require ample training before usage. Castellini et al. [48] and Yang et al. [51],

in two distinct studies, estimated forces using artificial neural networks (ANN), support vectors machines (SVM) and locally weighted projection regression (LWPR). Yang concluded that SVM outperforms ANN and LWPR.

Needle electromyography (NEMG) signals have been used to develop cross-subject force estimation models [52]. A cross-subject model preserves its accuracy across a variety of individuals. In other words, a model calibrated to one individual can be used to accurately estimate forces of another individual. However, NEMG involves inserting needles into the subject's muscles, a procedure that not only causes great discomfort, but also requires the presence of a trained professional and therefore it is not practical to use NEMG signals for controlling assistive devices. On the other hand, the best cross-subject correlation attained by SEMG estimation models to date is 0.6 [48]. Castellini et al. concluded that the models calibrated using SEMG signals from one individual could not be reliably used to estimate forces for another individual. Wang et al. concluded that SMEG-based torque estimation models tailored to one person are not applicable to other individuals. They also comment that the calibrated models for the same individual should not be used the next day. The models need to mathematically represent the underlying anatomy and physiology as individuals have different anatomy and muscle strength [53]. Therefore, it is important to calibrate models to individuals in order to capture the subject-specific physiological characteristics.

An experimental protocol is proposed and SEMG and torque data are gathered from healthy volunteers. This work intends to quantify the performance

of above-mentioned joint torque estimation models using the experimental data. The wrist joint was chosen as its functionality is frequently impaired due to aging [54] and stroke [33], and robots (controlled by SEMG signals) are developed to train and assist affected patients. Performance of six models for estimation of isometric wrist flexion and extension torques are compared: a physiological based model (PBM), an ordinary least squares linear regression model (OLS), a regularized least squares linear regression model (RLS), and three machine learning models, namely SVM, ANN, and LWPR. The second part of this work focuses on proving the viability of a model with high accuracy, short training time, and low sensitivity to alteration of arm configurations based on the results attained in the first part. The proposed methodology can potentially be used for controlling assistive devices after training models with data gathered from the patient.

CHAPTER 3 JOINT TORQUE ESTIMATION MODELS

3.1 Physiological Based Model

Physiological based model (PBM) used in this work is a neuromusculoskeletal model used for estimation of joint torques from SEMG signals. Processed SEMG signals are poor estimators of muscle forces [55, 56]. This is mainly due to (a) existence of a delay between SEMG and muscle tension onset (electromechanical delay) and (b) the fact that SEMG signals have a shorter duration than resulting forces. Muscle twitch response is modeled well by using a critically damped linear second order differential equation [57]. However, since SEMG signals are generally acquired at discrete time intervals, it is appropriate to use a discretized form. Using backward differences, the differential equation takes the form of a discrete recursive filter [58]:

$$u_j(t) = \alpha e_j(t-d) - \beta_1 u_j(t-1) - \beta_2 u_j(t-2) \quad (3\text{-}1)$$

where e_j is the processed SEMG signal of muscle j at time t, d is the electromechanical delay, α is the gain coefficient, $u_j(t)$ is the post-processed SEMG signal at time t, and β_1 and β_2 the recursive coefficients for muscle j.

Electromechanical delay was allowed to vary between 10 and 100 ms as that is the range for skeletal muscles [59]. The recursive filter maps SEMG values $e_j(t)$ for muscle j into post-processed values $u_j(t)$. Stability of this equation is ensured by satisfying the following constraints [60]:

$$\beta_1 = C_1 + C_2$$
$$\beta_2 = C_1 \times C_2$$
$$|C_1| < 1$$
$$|C_2| < 1 \qquad (3\text{-}2)$$

where C_1 and C_2 change the impulse response of the second-order filter.

When both these values are positive, an under-damped response is created. However, when both are negative or have different signs with $|C_1|>|C_2|$, the filter has a damped response. The damped response stretches the duration of the SEMG signal and the electromechanical delay (represented by d in 3-5) synchronizes activation and force production.

Unstable filters will cause $u_j(t)$ values to oscillate or even go to infinity. To restrict the maximum neural activation values to one, another constraint is imposed:

$$\alpha - \beta_1 - \beta_2 = 1 \qquad (3\text{-}3)$$

Neural activation values are conventionally restricted to values between zero and one, where zero implies no activation and one translates to full voluntary activation of the muscle.

Although isometric forces produced by certain muscles exhibit linear relationship with activation, nonlinear relationships are observed for other muscles. Nonlinear relationships are mostly witnessed for forces of up to 30% of the maximum isometric force [61]. These nonlinear relationships can be

associated with exponential increases in firing rate of motor units as muscle forces increase [62]. The exponential relationship can be modeled using the following equation:

$$a_j(t) = \frac{e^{Au_j(t)} - 1}{e^A - 1} \tag{3-4}$$

where A is called the non-linear shape factor. A=-3 corresponds to highly exponential behaviour of the muscle and A=0 corresponds to a linear one.

Once nonlinearities are explicitly taken into account, isometric forces generated by each muscle at neutral joint position at time t are computed using [63]:

$$F_j(t) = F_{max,j} \times a_j(t) \tag{3-5}$$

where $F_{max,j}$ is the maximum voluntary force produced by muscle j.

Isometric joint torque is computed by multiplying isometric force of each muscle by its moment arm:

$$\tau_j(t) = F_j(t) \times MA_j \tag{3-6}$$

where MA_j is moment arm at neutral wrist position for muscle j and $\tau_j(t)$ is the torque generated by muscle j at time t. Moment arms for flexors and extensors were assigned positive and negative signs respectively to maintain consistency with measured values.

As not all forearm muscles were accessible by surface electrodes (see Section 4.1 for details), each SEMG channel was assumed to represent intermediate and deep muscles in its proximity in addition to the surface muscle it was recording from. Torque values from each channel were then scaled using mean physiological cross-section area (PCSA) values tabulated by Jacobson et al. and Lieber et al. [64-66]. PCSA is defined as the total area of the cross-sections perpendicular to muscle fibres. Joint torque estimation values have been shown not to be highly sensitive to muscle PCSA values and therefore these values were fixed and not a part of model calibration [67]. The isometric torque at the wrist joint was computed by adding individual scaled torque values:

$$\tau_e(t) = \sum_{j=1}^{M} \frac{\sum \mathrm{PCSA_j}}{\mathrm{PCSA_j}} \times \tau_j(t) \tag{3-7}$$

where M is the number of muscles used in the model, and $\Sigma PCSA_j$ is the summation of PCSA of the muscle represents by muscle j and PCSA of muscle j itself.

Extensor Digitorum Communis (EDC), Extensor Carpi Ulnaris (ECU), Extensor Carpi Radialis Brevis (ECRB), Palmaris Longus (PL), and Flexor Digitorum Superficialis (FDS) represented extensor digiti minimi (EDM), extensor indicis proprius (EIP), extensor pollicis longus (EPL), flexor pollicis longus (FPL), and flexor digitorum profundus (FDP) respectively due to their anatomical proximity [68]. Abductor pollicis longus (APL) and extensor pollicis brevis (EPB) contribute negligibly to wrist torque generation due to their small moment arms

and were not considered in the model [69]. Steps and parameters involved in the PBM are summarized in Figure 3-1.

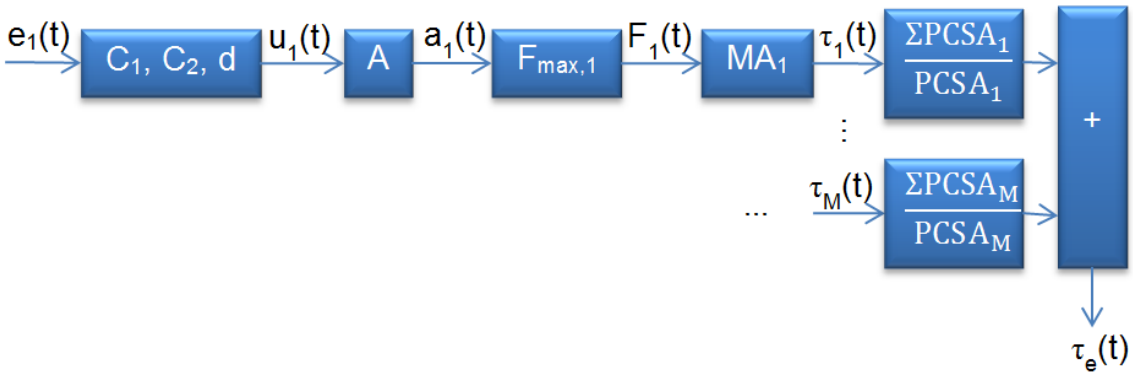

Figure 3-1: Steps and parameters involved in the PBM.

Models were calibrated to each volunteer by tuning model parameters. Yamaguchi [70] has summarized maximum isometric forces reported by different investigators. We used means as initial values and constrained F_{max} to one standard deviation of the reported values. Initial values for moment arms were fixed to the mean values in [71], and constrained to one standard deviation of the values reported in the same reference. Since these parameters are constrained within their physiologically acceptable values, calibrated models can potentially provide physiological insight [50]. Activation parameters A, C_1, C_2, and d were assumed to be constant for all muscles a model with too many parameters loses its predictive power due to overfitting [72]. Parameters x={A, C_1, C_2, d, $F_{max,1}$, …, $F_{max,M}$, MA_1, MA_2, …, MA_M} were tuned by optimizing the following objective function while constraining parameters to values mentioned beforehand:

$$\min_{x} [\tau_e(t) - \tau_m(t)]^2 \quad (3\text{-}8)$$

Models were optimized by Genetic Algorithms (GA) using MATLAB Global Optimization Toolbox (details of GA implementation are available in [73]). GA has previously been used for tuning muscle models [46]. Default MATLAB GA parameters were used and models were tuned in less than 100 generations [74].

3.2 Ordinary Least Squares Linear Regression Model

Linear regression model is a suitable tool for estimation of isometric joint torques using processed SEMG signals (SEMG signal processing will be presented in Section 4.3) [49]. Linear regression is presented as:

$$[\tau_m]_{N\times 1} = [\mathrm{SEMG}]_{N\times M}[\beta]_{M\times 1} + [\epsilon]_{N\times 1} \quad (3\text{-}9)$$

where N is the number of samples considered (observations), M is the number of muscles, τ_m is a vector of measured torque values, SEMG is a matrix of processed SEMG signals, β is a vector of regression coefficients to be estimated, and ε is a vector of independent random variables.

Ordinary least squares (OLS) method is most widely used for estimation of regression coefficients [51]. Estimated vector of regression coefficients using least squares method ($\hat{\beta}$) is computed using:

$$\hat{\beta} = \left[[\mathrm{SEMG}]^T[\mathrm{SEMG}]\right]^{-1}[\mathrm{SEMG}]^T[\tau_m] \quad (3\text{-}10)$$

Once the model is fitted, SEMG values can be used for estimation of torque values (τ_e) as shown:

$$[\tau_e]_{N\times 1} = [SEMG]_{N\times M}\hat{\beta}_{M\times 1} \quad (3\text{-}11)$$

3.3 Regularized Least Squares Linear Regression Model

The ℓ_1-regularized least squares (RLS) method for estimation of regression coefficients overcomes the estimation accuracy and interpretation issues that are associated with the ordinary least squares method [75]. Estimated vector of regression coefficients using ℓ_1-regularized least squares method ($\hat{\beta}$) is computed through the following optimization:

$$\text{minimize} \sum_{i=1}^{N}\left([SEMG]_{N\times M}[\hat{\beta}]_{M\times 1} + [\epsilon]_{N\times 1} - [\tau_m]_{N\times 1}\right)^2 + \sum_{i=1}^{M}\lambda|\hat{\beta}_i| \quad (3\text{-}12)$$

where $\lambda \geq 0$ is the regularization parameter which is generally set equal to 0.01 [76, 77].

We used the MATLAB implementation of the ℓ_1-regularized least squares method [78].

3.4 Support Vector Regression

Support vectors machines (SVM) are machine learning methods used for classification and regression. Support vector regression (SVR) maps input data using a non-linear mapping to a higher-dimensional feature space where linear regression can be applied. Unlike neural networks, SVR does not suffer from the local minima problem since model parameter estimation involves solving a convex optimization problem [79].

We used epsilon support vector regression (ε-SVR) available in the LibSVM tool for MATLAB [80]. Details of ε-SVR problem formulation are available in Appendix B and [81]. ε-SVR has previously been utilized for estimation of grasp forces [48, 51]. The Gaussian kernel was used as it enables nonlinear mapping of samples and has a low number of hyperparameters, which reduces complexity of model selection [82]. Eight-fold cross-validation to generalize error values and grid-search for finding the optimal values of hyperparameters C and σ, and ε were carried out for each model.

3.5 Artificial Neural Networks

Artificial neural networks (ANN) have been used for SEMG classification and regression extensively [48, 51, 83, 84]. Three layer neural networks have been shown to be adequate for modeling problems of any degree of complexity [85]. We used feed-forward back propagation network with one input layer, two hidden layers, and one output layer [86]. We also used BFGS quasi-Newton training that is much faster and more robust than simple gradient descent [87]. Network structure is depicted in Figure 3-2, where M is the number of processed SEMG channels used as inputs to the ANN and τ_e is the estimated torque value.

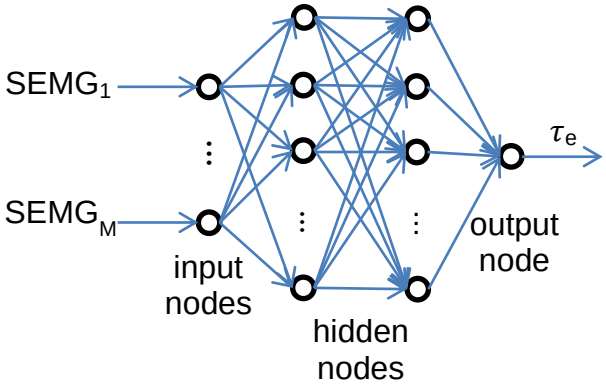

Figure 3-2: ANN Structure.

ANN models were trained using MATLAB Neural Network Toolbox. Hyperbolic tangent sigmoid activation functions were used to capture the nonlinearities of SEMG signals. For each model, the training phase was repeated ten times and the best model was picked out of those repetitions in order to overcome the local minima problem [79]. We also used early stopping and regularization in order to improve generalization and reduce the likelihood of overfitting [88]. More information about multiple-layer neural networks is available in Appendix C.

3.6 Locally Weighted Projection Regression

Locally Weighted Projection Regression (LWPR) is a nonlinear regression method for high-dimensional spaces with redundant and irrelevant input dimensions [89]. LWPR employs nonparametric regression with locally linear models based on the assumption that high dimensional data sets have locally low dimensional distributions. However piecewise linear modeling utilized in this

method is computationally expensive with high dimensional data (more details are available in Appendix D).

We used Radial Basis Function (RBF) kernel and meta-learning and then performed an eight-fold cross validation to avoid overfitting. Finally, we used grid search to find the initial values of the distance metric for receptive fields, as it is customary in the literature [48, 51]. Models were trained using a MATLAB version of LWPR [90].

CHAPTER 4 EXPERIMENTAL DATA

Eleven healthy volunteers (eight males, three females, age 25±4, mass 74±12kg, height 176±7cm), who signed an informed consent form (project approved by the Office of Research Ethics, Simon Fraser University; Reference # 2009s0304), participated in this study. As a first step, experiments were conducted using healthy volunteers in order to demonstrate the general applicability of the models explored in this study before testing these models on the data gathered from the elderly (future research).

A custom-built rig was designed to allow for measurement of isometric torques exerted about the wrist joint. Volunteers placed their palm on a plate and Velcro straps were used to secure their hand and forearm to the plate. The plate hinged about the axis of rotation shown in Figure 4-1.

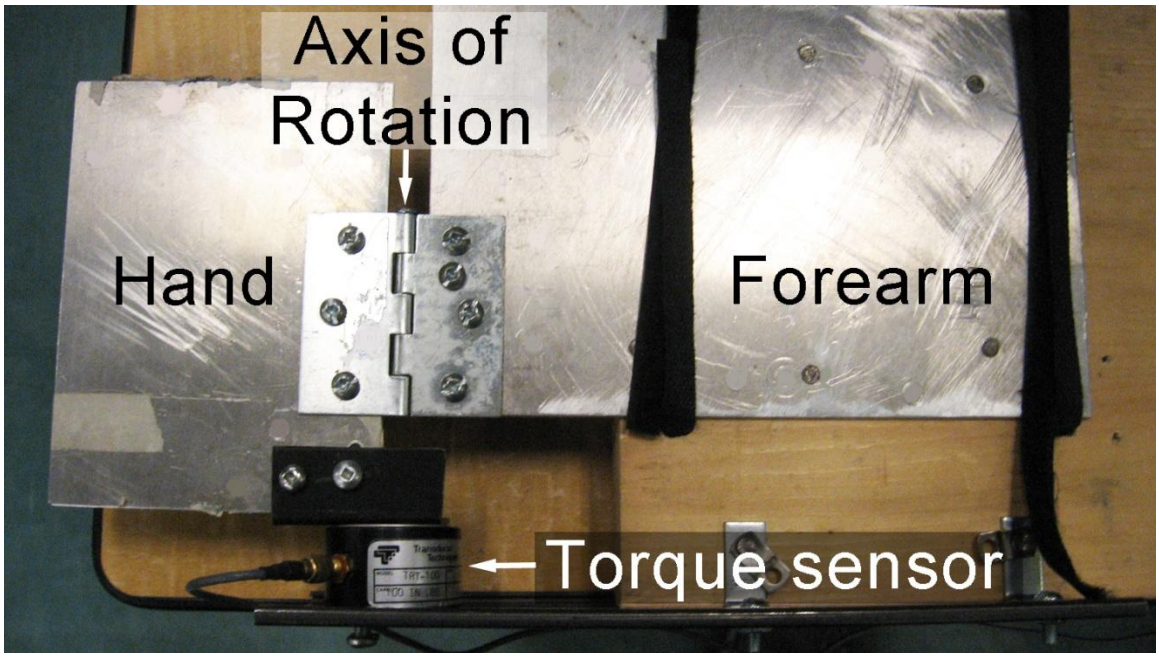

Figure 4-1: Custom-built rig equipped with a torque sensor

A Transducer Techniques TRX-100 reaction torque sensor was used to measure torques applied about the rig's axis of rotation. Volunteer's forearm was secured to the rig using two Velcro straps. This design allowed restriction of arm movements. Volunteer placed their elbow on the rig and assumed an upright position.

4.1 Data Collection Protocol

Each volunteer was asked to flex and then extend his right wrist with maximum voluntary contraction (MVC). MVC is defined as the maximum torque that can be generated by the muscles spanning a joint at a fixed joint angle. Once the MVC values for both flexion and extension were determined, the

volunteer was asked to gradually flex her/his wrist to 50% of MVC. Once the 50% was reached the volunteer gradually decreased the exerted torque to zero. This procedure was repeated three times for flexion and then for extension. Finally, the volunteer was asked to flex and extend her/his wrist to 25% of MVC three times. These values were selected in order to prevent the overexertion and fatigue of the volunteers' muscles that are known to change the SEMG signal characteristics [91]. Figure 4-2 shows a sample of torque signals gathered. Positive values on the scale are for flexion and negative values are for extension.

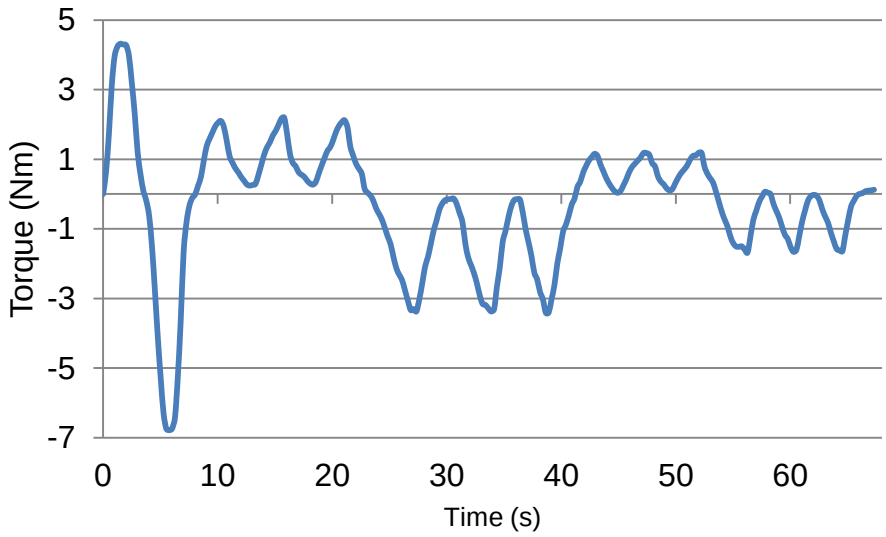

Figure 4-2: Sample torque signal.

Following the completion of this protocol, volunteers were asked to supinate their forearm, and follow the same protocol as before. Forearm is supinated when the palm faces up whereas it is the pronated when the palm faces down. Figure 4-3 shows forearm in pronated and supinated positions.

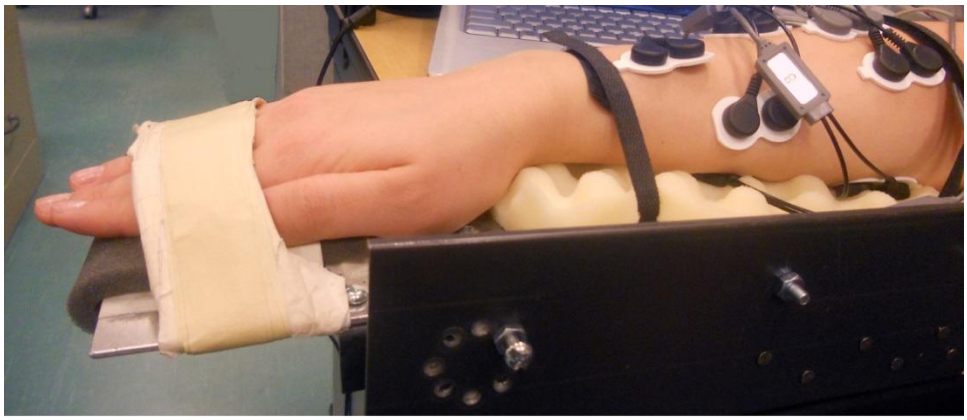

(a)

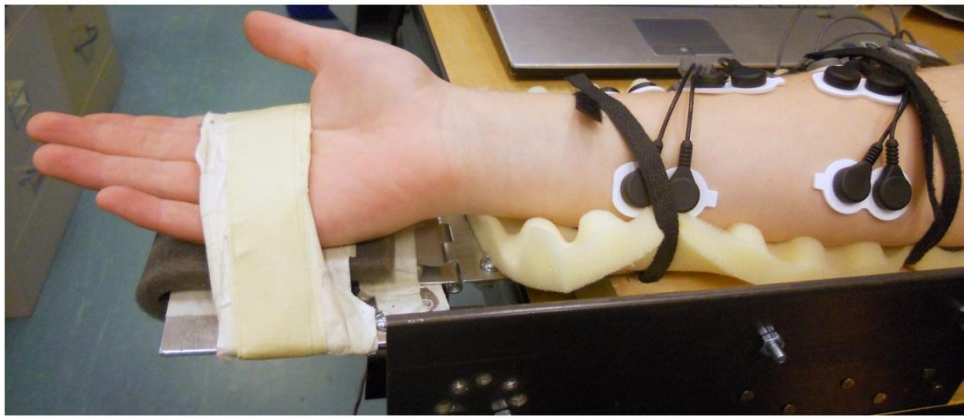

(b)

Figure 4-3: Volunteer's forearm on the testing rig.

(a) Forearm pronated, (b) Forearm supinated.

Completion of protocols in both pronated and supinated forearm positions was called a session. Table 4-1 summarizes actions in protocols.

Table 4-1: Actions and repetitions for protocols.

Repetition	Action
1	Wrist flexion with maximum torque
1	Wrist extension with maximum torque
3	Gradual wrist flexion until 50% MVC and gradual decrease to zero
3	Gradual wrist extension until 50% MVC and gradual decrease to zero
3	Gradual wrist flexion until 25% MVC and gradual decrease to zero
3	Gradual wrist extension until 25% MVC and gradual decrease to zero

In order to capture the effects of passage of time on model accuracy, volunteers were asked to repeat the same session after one hour. This session was named session two. Electrodes were not detached in between the two sessions. After completion of session two, electrodes were removed from the volunteer's skin. The volunteer was asked to repeat another session in twenty-four hours following session two while attaching new electrodes. This was intended to capture the effects of electrode displacement and further time passage.

Each volunteer was asked to supinate her/his forearm and exert isometric torques on the rig following the same protocol used before after completion of session 1. This was intended to study the effects of arm configurations on model accuracy.

4.2 SEMG Acquisition

A commercial SEMG acquisition system (Noraxon Myosystem 1400L) was used to acquire signals from eight SEMG channels. Each channel was connected to a Noraxon AgCl gel dual electrode that picked up signals from the muscles tabulated in Table 4-2.

Table 4-2: Muscles monitored using SEMG.

Channel	Muscle	Action
1	Extensor Carpi Radialis Longus (ECRL)	Wrist extension
2	Extensor Digitorum Communis (EDC)	Wrist extension
3	Extensor Carpi Ulnaris (ECU)	Wrist extension
4	Extensor Carpi Radialis Brevis (ECRB)	Wrist extension
5	Flexor Carpi Radialis (FCR)	Wrist flexion
6	Palmaris Longus (PL)	Wrist flexion
7	Flex or Digitorum Superficialis (FDS)	Wrist flexion
8	Flexor Carpi Ulnaris (FCU)	Wrist flexion

Forearm has fifteen extrinsic muscles that are responsible for moving the wrist and the fingers. However, only eight muscles are superficial muscles and the rest cannot be monitored using SEMG. It has been reported that the extrinsic muscles of the forearm have large torque generating contributions in isometric flexion and extension [92]. Therefore, we considered three superficial secondary forearm muscles as well as the primary forearm muscles accessible via SEMG. The skin preparation procedure outlined in surface electromyography for the non-invasive assessment of muscles project (SENIAM) was followed to maximize

SEMG signal quality [93]. Figure 4-4 shows the position of electrodes attached to a volunteer's forearm.

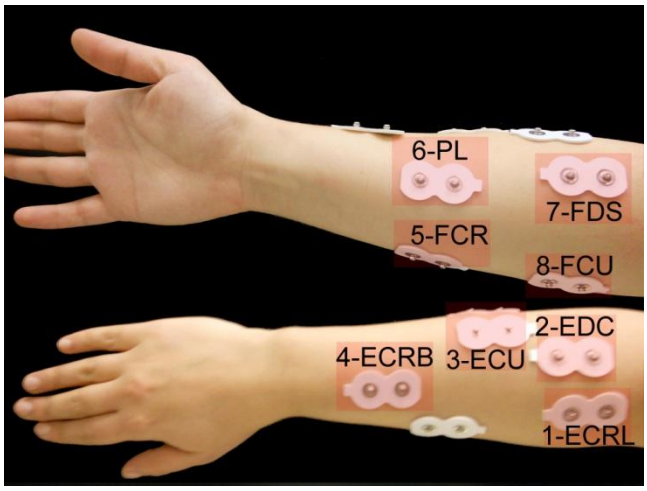

Figure 4-4: Electrode positions.

SEMG signals were acquired at 1kHz using a National Instruments (NI-USB-6289) data acquisition card. An application was developed using LabVIEW software that stored data on a computer and provided visual feedback for volunteers. Visual feedback consisted of a bar chart that visualized the magnitude of exerted torques, which aided volunteers to follow the protocol more accurately.

4.3 Signal Processing

Initially DC offset values of SEMG signals were removed. Signals were subsequently high-pass filtered using a zero-lag Butterworth fourth order filter (30Hz cut-off frequency), in order to remove high-frequency noise and avoid aliasing. Signals were then low-pass filtered using a zero-lag Butterworth fourth

order filter with 6Hz cut-off frequency (in order to remove the motion artefact), full-wave rectified, and normalized to the maximum SEMG value for each channel [53]. Figure 4-5 shows the signal processing scheme.

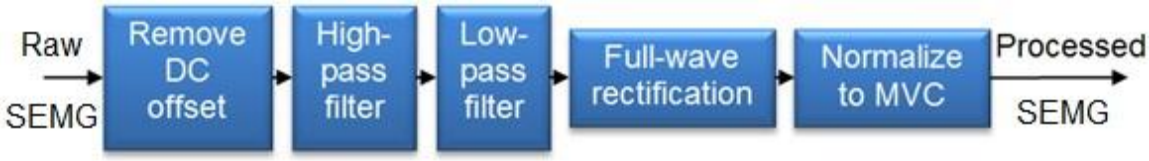

Figure 4-5: SEMG signal processing scheme.

33,520 samples were acquired from each of the eight SEMG channels and the torque sensor for each volunteer. The data set was broken down into training and testing data. Figure 4-6 shows a sample of raw and processed SEMG signals.

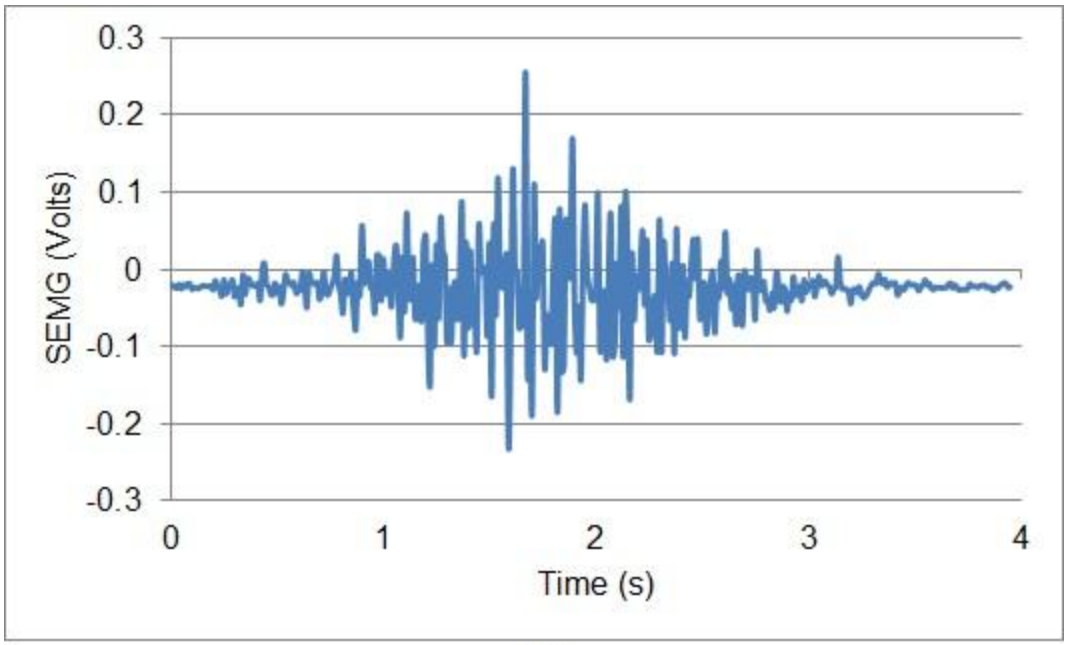

(a)

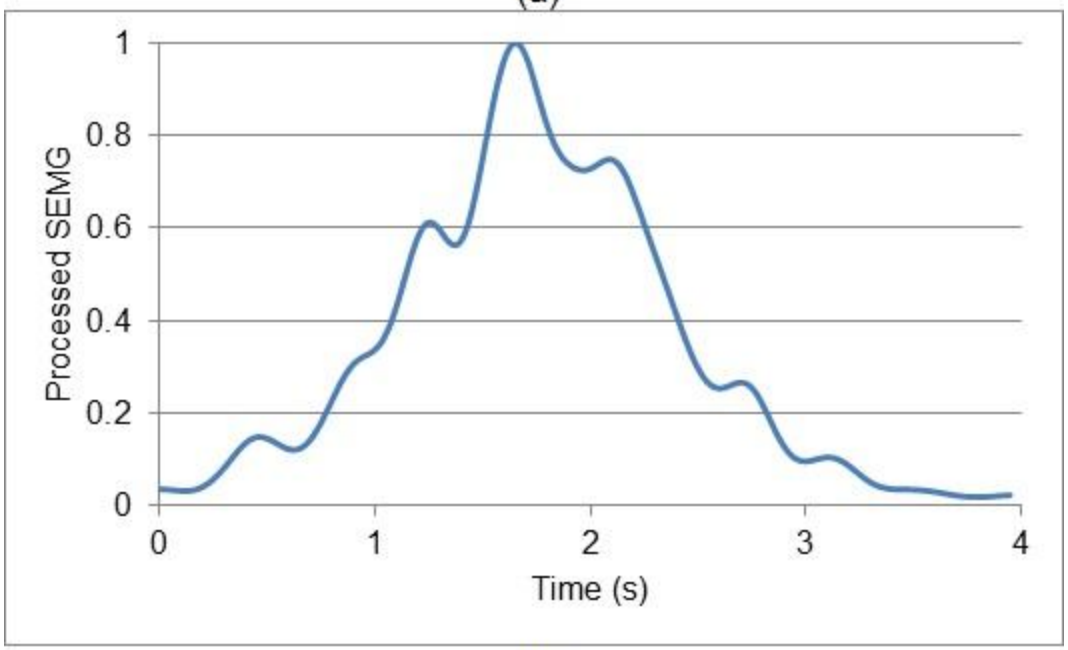

(b)

Figure 4-6: Sample SEMG signal.

(a) Raw, (b) processed.

CHAPTER 5 COMPARISON OF MODEL PERFORMANCE

Models were initially trained with the training data set. Training, in this context, refers to the process of finding the coefficient of regression for linear regression models and tuning the physiological parameters for the PBM using the training data set. The performance of trained models was subsequently tested by comparing estimated torque values from the model and the actual torque values from the testing data set. Two accuracy metrics were used to compare the performance of different models. The first metric, normalized root mean squared error (NRMSE) is a measure of model accuracy while the second metric, adjusted coefficient of determination (R^2) is a measure of how future outcomes are likely to be estimated in the future [94]. Root mean squared error (RMSE) is a measure of the difference between measured and estimated values. NRMSE is a dimensionless metric expressed as RMSE over the range of measured torques values for each volunteer:

$$\mathrm{NRMSE} = \frac{\sqrt{\frac{\sum_{i=1}^{n}\left(\tau_e(i) - \tau_m(i)\right)^2}{n}}}{\tau_{m,flex} - \tau_{m,ext}} \tag{5-1}$$

where $\tau_e(i)$ is the estimated and $\tau_m(i)$ is the measured torque value for sample i, n corresponds to the total number of samples tested, and $\tau_{m,flex}$ and $\tau_{m,ext}$ are the maximum flexion and extension torques exerted by each volunteer.

Unadjusted coefficient of determination (R_u^2) is a measure of the percentage of variation in the dependant variable (torque) collectively explained by the independent variables (SEMG signals):

$$R_u^2 = 1 - \frac{\sum_{i=1}^{n}(\tau_e(i) - \tau_m(i))^2}{\sum_{i=1}^{n}(\tau_m(i) - \bar{\tau}_m)^2} \quad (5\text{-}2)$$

where $\bar{\tau}_m$ is the mean measured torque.

However R_u^2 has a tendency to overestimate the regression as more independent variables are added to the model. For this reason, many researchers recommend adjusting R^2 for the number of independent variables [94]:

$$R^2 = 1 - \left[\left(\frac{n-1}{n-k-1}\right) \times (1 - R_u^2)\right] \quad (5\text{-}3)$$

where R^2 is the adjusted coefficient of determination, n is the number of samples and k is the number of SEMG channels.

Models were trained using every 100 data resampled from the processed signals to save model training time. Data set was reduced from 33,520 to 335 samples with resampling. Training time t, was measured as the number of seconds it took for each model to be trained. Resampling the data originally sampled at 1000Hz at every 100 samples effectively translated to data samples that were 100 ms apart. A delay of 200 ms is the maximum delay tolerated by users of assistive devices and therefore a suitable controller should be able to generate control signals with a 100 ms delay [26]. All training and testing was

performed on a computer with an Intel® CoreTM2 Duo 2.5GHz processor and 6GB of RAM. Table 5-1 compares mean training times for models trained using the original and resampled data sets.

Table 5-1: Model training times for original and resampled data sets.

Time (s)	PBM	OLS	RLS	SVM	ANN	LWPR
Original	1,080.07	0.01	1.98	19,125.31	166.73	5,195.03
Resampled	10.96	0.00	0.03	15.32	9.40	18.63

One-way Analysis of Variance (ANOVA) failed to reject the null hypothesis that NRMSE and R^2 have different mean values for each model, meaning that the difference between means is not significant (with minimum P-value of 0.95). We used reduced data sets with data resampled every 100 samples for the rest of the study (Appendix E details the procedure for one-way ANOVA test).

5.1 Effects of Number of Muscles

As merely one degree of freedom of the wrist was considered in this study, the possibility of training models using only two primary muscles was investigated initially. There are six combinations possible with one primary flexor and one primary extensor muscle: FCR-ECRL, FCR-ECRB, FCR-ECU, FCU-ECRL, FCU-ECRB, and FCU-ECU. Models were trained using 75% of the data for all six combinations and then tested on the remaining 25% and the model with the best performance was picked. Mean and standard deviation of NRMSE and

R^2 for models trained with two, five, and eight channels are presented in Table 5-2.

Table 5-2: Torque estimation for models trained with 2, 5, and 8 SEMG channels.

Model		8 channels		5 channels		2 channels	
		NRMSE	R^2	NRMSE	R^2	NRMSE	R^2
PBM	Mean	2.73%	0.85	3.07%	0.86	4.59%	0.77
	STD	0.97%	0.13	1.03%	0.11	1.32%	0.19
OLS	Mean	2.88%	0.82	3.17%	0.77	4.82%	0.63
	STD	0.94%	0.11	1.06%	0.13	1.81%	0.23
RLS	Mean	2.83%	0.82	3.11%	0.79	4.73%	0.69
	STD	0.93%	0.10	1.01	0.11	1.31%	0.18
SVM	Mean	2.85%	0.82	3.00%	0.80	4.77%	0.73
	STD	1.00%	0.09	1.04%	0.10	1.02%	0.14
ANN	Mean	2.82%	0.82	3.03%	0.81	4.74%	0.69
	STD	0.95%	0.09	1.05%	0.12	1.17%	0.18
LWPR	Mean	3.03%	0.75	3.19%	0.78	4.97%	0.69
	STD	1.14%	0.21	1.19%	0.13	1.31%	0.21

It is noteworthy that best performance was not consistently attributed to a single combination of muscles for the case of models trained with two channels. It is evident that models trained with five channels are superior to models trained with two. However models trained with eight channels do not have significant performance superiority. Figure 5-1 compares NRMSE and R^2 for different number of training channels.

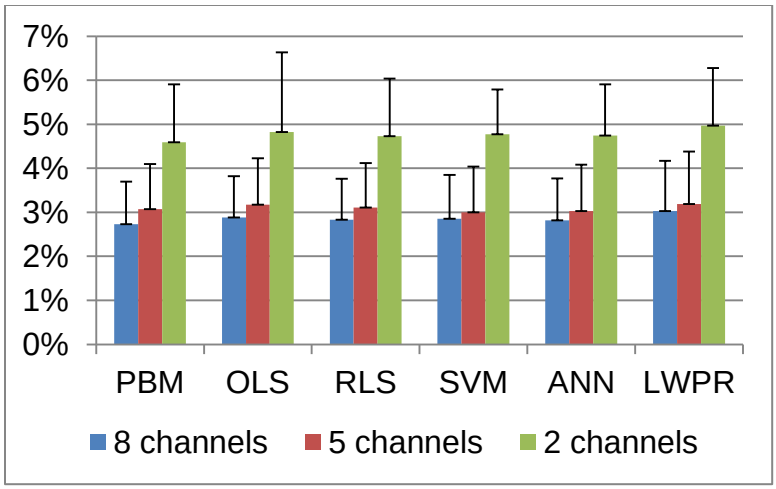

(a)

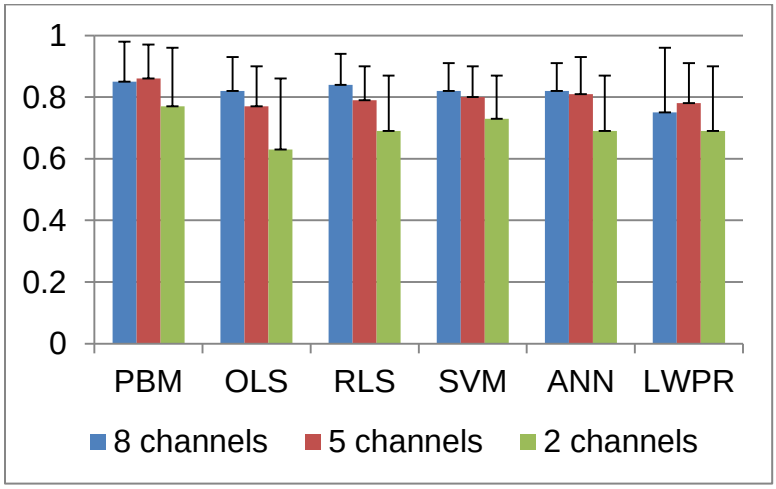

(b)

Figure 5-1: Effects of the number of SEMG channels on torque estimation. (a) NRMSE, (b) R^2.

This result appears to be in contrast to the results obtained by Delp et al. [92] where extrinsic muscles of the hand are expected to contribute substantially to torque generation. However, due to the design of our testing rig, volunteers

only generated torque by pushing their palms against the torque-sensing plate and their fingers did not contribute to torque generation. Therefore, the addition of SEMG signals of extrinsic muscles to the model did not result in a significant increase in accuracy.

It should be noted that using more data for training models increases accuracy for same session models. Table 5-3 compares NRMSE and R^2 for two extreme cases where 25% and 90% of the data set is used for training models and the rest of the data set is used for testing using all SEMG channels.

Table 5-3: Comparison of training data set size on joint torque estimation.

Model		**25% training**		**90% training**	
		NRMSE	R^2	NRMSE	R^2
PBM	Mean	4.41%	0.81	2.32%	0.96
	STD	2.49%	0.09	0.59%	0.04
OLS	Mean	4.19%	0.80	2.19%	0.97
	STD	2.19%	0.10	0.58%	0.04
RLS	Mean	4.14%	0.82	2.07%	0.97
	STD	2.13%	0.08	0.51%	0.03
SVM	Mean	4.39%	0.85	2.02%	0.97
	STD	2.46%	0.09	0.92%	0.03
ANN	Mean	5.87%	0.73	2.34%	0.96
	STD	2.20%	0.20	0.61%	0.03
LWPR	Mean	6.41%	0.69	3.43%	0.87
	STD	3.14%	0.29	0.84%	0.07

Mean R^2 values increased 19%, 21%, 18%, 14%, 32%, and 26% while mean NRMSE values decreased 47%, 48%, 50%, 54%, 60%, and 46% for PBM,

OLS, RLS, SVM, ANN, and LWPR, respectively. Figure 5-2 visualizes NRMSE and R^2 for the two cases.

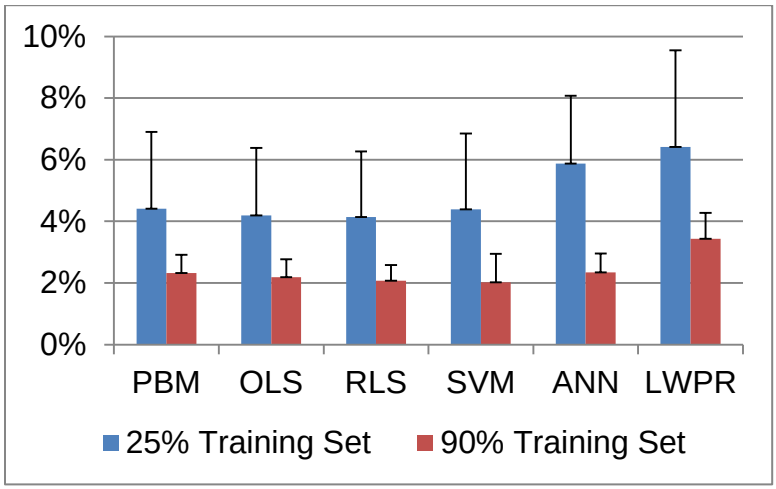

(a)

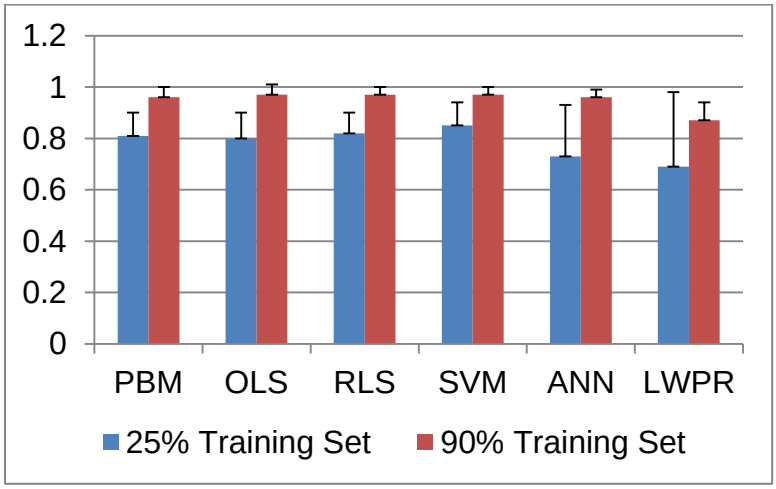

(b)

Figure 5-2: Comparison of training data set size on joint torque estimation. (a) NRMSE, (b) R^2.

The percentage of the data set used for model training is merely relevant for allowing a fair comparison between models trained with different number of SEMG channels. Irrespective of the percentage of data used for training, model accuracy increases with increasing the number of SEMG channels.

For PBM training with two and five channels, ΣPCSA term in Equation 3-10 was modified. For the two channel case, equation 5-4 took the following form:

$$\tau_e(t) = \frac{\sum \mathrm{PCSA}_{\mathrm{flexors}}}{\mathrm{PCSA}_{\mathrm{flexor}}} \times \tau_{\mathrm{flexor}}(t) + \frac{\sum \mathrm{PCSA}_{\mathrm{extensors}}}{\mathrm{PCSA}_{\mathrm{extensor}}} \times \tau_{\mathrm{extensor}}(t) \qquad (5\text{-}4)$$

where $\Sigma PCSA_{flexors}$ is the summation of PCSA of all flexor muscles, $\Sigma PCSA_{extensors}$ is the summation of PCSA of all extensor muscles, $PCSA_{flexor}$ is the PCSA of the flexor muscle used for training, $PCSA_{extensor}$ is the PCSA of the extensor muscle used for training, $\tau_{flexor}(t)$ is the torque of the flexor muscle used for training at time t, and $\tau_{extensor}(t)$ is the torque of the flexor muscle used for training at time t.

Similarly, PBM training with the five primary wrist muscles was carried out with modified ΣPCSA terms. Half of the summation of PCSA values for non-primary flexors was added to each of the two primary flexors while a third of the summation of PCSA values for non-primary extensors was added to the ΣPCSA term of each of the three primary extensors.

These modifications allowed tuned parameters to stay within their physiologically acceptable values, even though less SEMG channels were used for training models.

5.2 Cross Session Analysis

Passages of time as well as electrode displacement adversely affect accuracy of models trained with SEMG [46, 49]. Models trained with session 1 were tested with data from session 2 (in one hour without detaching electrodes) and session 3 (in twenty-four hours and with new electrodes attached). Table 5-4 compares model performance for the two cases.

Table 5-4: Effects of passage of time and electrode displacement on joint torque estimation.

Model		After 1 hour		After 24 hours	
		NRMSE	R^2	NRMSE	R^2
PBM	Mean	5.28%	0.56	5.54%	0.47
	STD	2.68%	0.24	2.95%	0.26
OLS	Mean	4.84%	0.59	5.29%	0.51
	STD	2.98%	0.27	3.04%	0.25
RLS	Mean	4.81%	0.63	5.19%	0.54
	STD	2.91%	0.23	2.98%	0.27
SVM	Mean	5.35%	0.54	6.76%	0.46
	STD	2.22%	0.21	2.95%	0.28
ANN	Mean	5.40%	0.53	6.44%	0.51
	STD	2.15%	0.28	3.09%	0.31
LWPR	Mean	5.42%	0.60	5.93%	0.59
	STD	3.00%	0.23	3.18%	0.30

Results suggest that model reliability deteriorates with passage of time. This phenomena can be mainly attributed to the changes in SEMG signal characteristics as a result of changing electrical characteristics of the skin due to

sweating or changes in humidity [40], and has been observed in other studies [48, 91]. Figure 5-3 compares mean and standard deviation of NRMSE and R^2 of models trained with session 1 and tested with data from the same session, after one and twenty-four hours.

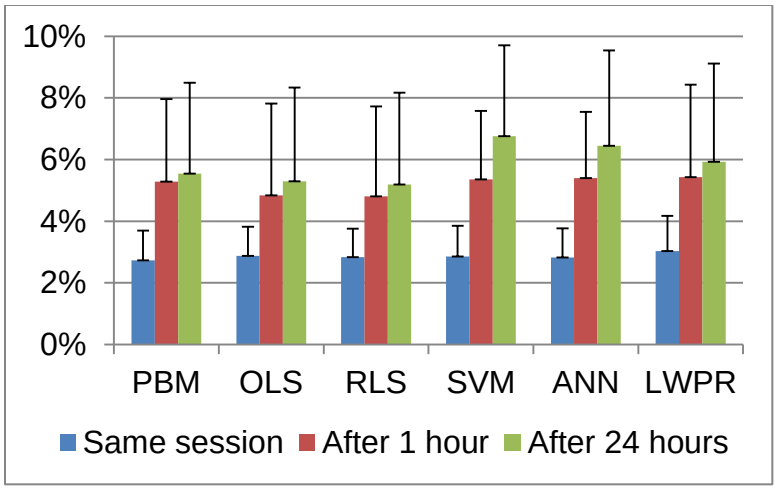

(a)

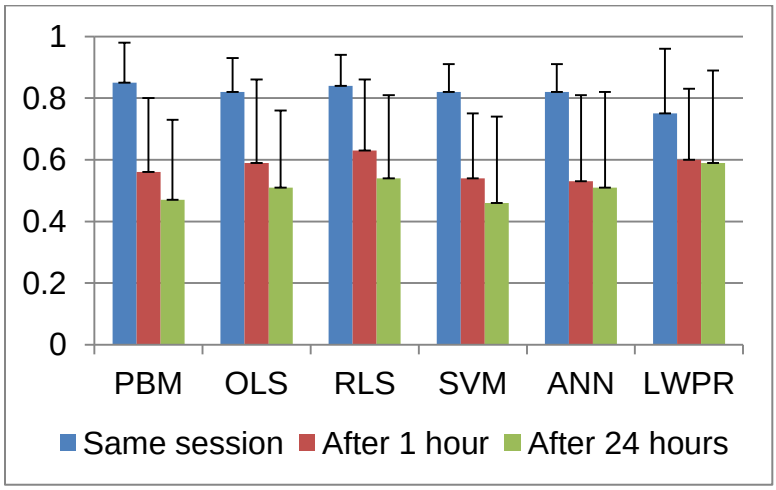

(b)

Figure 5-3: Effects of passage of time and electrode displacement on joint torque estimation.

(a) NRMSE, (b) R^2.

Mean R^2 values after one hour decreased 34%, 28%, 25%, 34%, 35%, and 20% while mean NRMSE decreased 93%, 68%, 70%, 88%, 91%, and 79%

for PBM, OLS, RLS, SVM, ANN, and LWPR, respectively. After twenty-four hours mean NRMSE values decreased further. High standard deviations of NRMSE and R^2 values suggest unreliability of model estimations with passage of time and electrode displacement. Therefore, it is crucial for models trained using SEMG signals to be retrained frequently regardless of the model utilized.

5.3 Effects of Arm Configurations Alterations

Arm configurations changes SEMG signal characteristics. These changes are primarily a result of a shift of muscles with respect to electrodes [39]. A model trained with the forearm in pronated position was utilized to predict the measured values from the supinated position in the same session. Supinating the forearm resulted in the torque sensor readings for extension and flexion to be reversed. This was explicitly taken into account when processing signals. Estimation accuracy of the trained models reduced significantly with forearm supination as shown in Table Table 5-5.

Table 5-5: Effects of forearm supination on joint torque estimation.

Model		NRMSE	R^2
PBM	Mean	9.55%	0.22
	STD	5.69%	0.32
OLS	Mean	8.93%	0.25
	STD	5.37%	0.33
RLS	Mean	8.86%	0.23
	STD	5.30%	0.29
SVM	Mean	8.65%	0.24
	STD	4.47%	0.37
ANN	Mean	9.13%	0.23
	STD	4.76%	0.36
LWPR	Mean	10.05%	0.25
	STD	5.49%	0.30

ANOVA shows that the NRMSE and R^2 of testing for the two cases are significantly different ($P<0.01$). Results from this experiment validate that trained models are very sensitive to arm configurations. Forearm supination shifts SEMG signal space. Since models trained in the pronated position do not take this shift into consideration, accuracy decreases [48]. SEMG patterns change with different arm configurations that models need to explicitly take into consideration [95, 96]. Figure 5-4 shows the effects of forearm supination on estimation accuracy of models trained with forearm in pronated position. Mean NRMSE values increased 2.50, 2.10, 2.13, 2.04, 2.24, and 2.32 times for PBM, OLS, RLS, SVM, ANN, and LWPR.

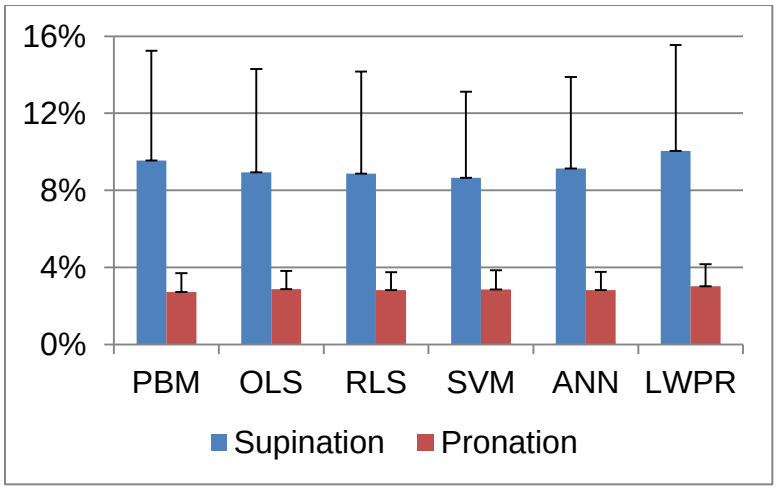

(a)

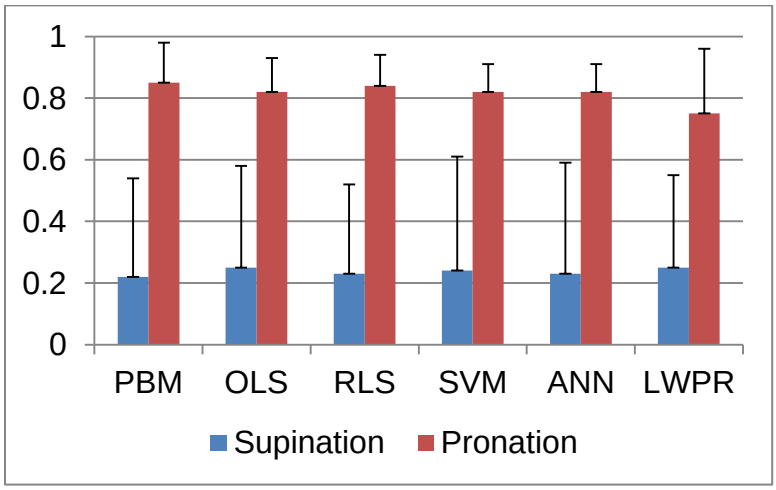

(b)

Figure 5-4: Effects of arm configurations on joint torque estimation.
(a) NRMSE, (b) R^2.

5.4 Comparison

Table 5-6 summarizes performance of models based on different criteria. One advantage of machine learning models (SVM, ANN, and LWPR) is that these models can be trained with raw SEMG signals, as they are capable of

mapping the nonlinearities associated with raw SEMG signals. In contrast, PBM can only be trained with processed SEMG signals since inputs to the PBM represent neural activity of muscles (a value bounded between zero and one) [53]. Moreover, nonlinear behaviour of muscles [36] observed in raw SEMG signals precludes utilization of linear regression for mapping.

Table 5-6: Comparison of models investigated.

Criteria	PBM	OLS	RLS	SVM	ANN	LWPR
Least training time		*				
Physiological insight	*					
Does not require SEMG processing				*	*	*
Supination sensitivity	*	*	*	*	*	*
Time passage sensitivity	*	*	*	*	*	*
Electrode placement sensitivity	*	*	*	*	*	*

CHAPTER 6 MODIFIED LINEAR REGRESSION MODEL

It was established in the preceding chapter that the performance of predictive models rapidly deteriorates with arm configurations alteration. The remedy to this issue is to explicitly train models under different arm configurations. In this section we consider a modified linear regression model with two additional inputs: wrist joint angle ($\theta_{\mathrm{Flex/Ext}}$) and forearm supination angle ($\theta_{\mathrm{Pro/Sup}}$). For the former input, neutral wrist position is set equal to 0°, wrist flexion is measured with a positive sense relative to the neutral position and wrist extension has a negative sense. For the latter input, forearm resting on the table in the pronated position was assigned 0°, and supination of the forearm was assigned was assigned 180°. Equation 5-5 mathematically represents the model.

$$\tau_{\mathrm{N}\times 1} = \mathrm{X}_{N\times 10}\beta_{10\times 1} + \epsilon_{\mathrm{N}\times 1}$$

$$\mathrm{X} = \begin{bmatrix} \mathrm{SEMG}_{1,1} & \dots & \mathrm{SEMG}_{8,1} & \theta_{\mathrm{Pro/Sup}_1} & \theta_{\mathrm{Flex/Ext}_1} \\ \vdots & & \vdots & \vdots & \vdots \\ \mathrm{SEMG}_{1,\mathrm{N}} & \dots & \mathrm{SEMG}_{8,\mathrm{N}} & \theta_{\mathrm{Pro/Sup}_\mathrm{N}} & \theta_{\mathrm{Flex/Ext}_\mathrm{N}} \end{bmatrix} \quad (6\text{-}1)$$

where N is the number of observations, τ is the isometric torque in Newton meters, $\mathrm{SEMG}_{i,j}$ is the processed SEMG signal where i is the muscle number and j is the observation, β is the vector of regression coefficients, and ε is a vector of independent random variables.

Each row in the X matrix represents all SEMG and angle data at one instant. Each column represents data from one of the channels (eight SEMG and two angle channels) for all observations.

Figure 6-1 depicts the structure of the modified linear regression model.

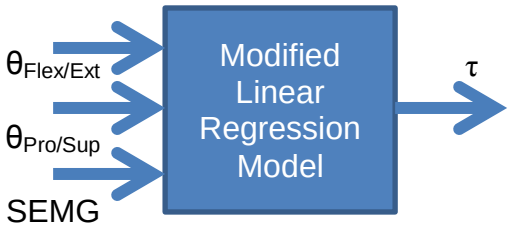

Figure 6-1: Modified linear regression model.

We used ℓ_1-regularized least squares method to compute the regression coefficients of the linear regression model as it overcomes the common issues associated with ordinary least squares method and provides higher estimation accuracy.

In order to test the performance of the model, four additional data sets were gathered from each volunteer. Volunteers were asked to flex and extend their wrists following the same protocol as before, with the rig fixed at different positions as shown in Figure 6-2.

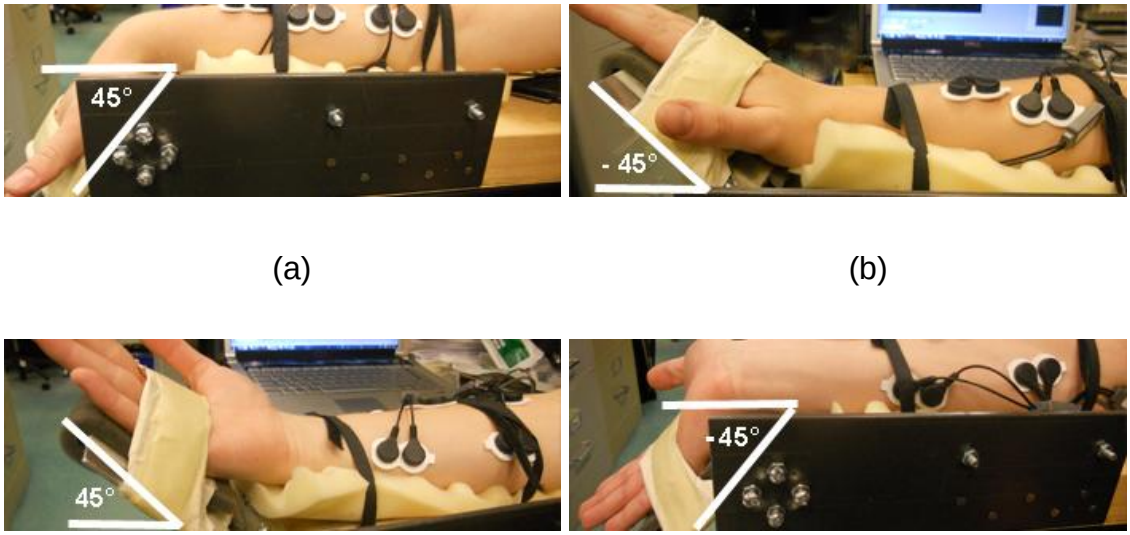

(a) (b)

(c) (d)

Figure 6-2: Forearm on the testing rig.

(a) Pronated and flexed 45°, (b) Pronated and extended 45°, (c) Supinated and flexed 45°, (d) Supinated and extended 45°.

Neutral wrist position represented zero degrees, wrist flexion was measured with a positive sense relative to the neutral position, and wrist extension was assigned a negative sense. Table 6-1 lists all the configurations.

Table 6-1: Arm configurations.

Configuration	Forearm position	Wrist flexion
1	Pronated	0°
2	Pronated	45°
3	Pronated	-45°
4	Supinated	0°
5	Supinated	45°
6	Supinated	-45°

First, we demonstrate the extent of model accuracy deterioration with varied joint angles and forearm supination. We trained a linear regression model with data gathered from configuration 1 (pronated forearm), and tested model accuracy with testing data from all six configurations. Table 6-2 demonstrates the results.

Table 6-2: Effects of wrist angle and forearm configurations variation on model accuracy

Configuration	NRMSE	R^2
1	2.82%±0.91%	0.84±0.10
2	3.53%±1.33%	0.58±0.25
3	3.90%±1.44%	0.61±0.29
4	8.93%±5.37%	0.25±0.33
5	10.32%±6.03%	0.17±0.37
6	10.44%±5.89%	0.15±0.39

Evidently, model accuracy drops significantly with supination of the forearm while varying wrist joint angles does not substantially affect model

accuracy. Figure 6-3 depicts the sharp variations of mean NRMSE and R^2 following forearm supination.

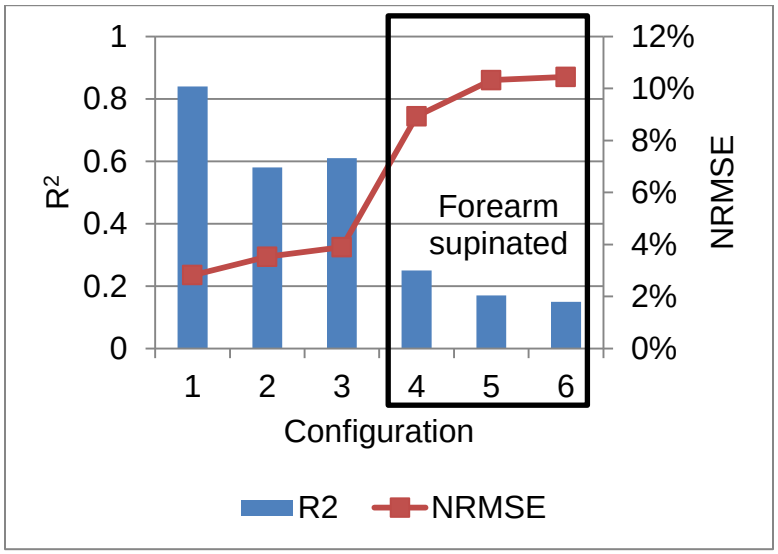

Figure 6-3: Accuracy deterioration with arm configurations and joint angle variations.

Supinating the forearm following training a model with pronated forearm causes a shift in SEMG input space that the model cannot take into account. Therefore, models need to be trained at all configurations that would result in an SEMG input space shift [40]. We demonstrate how training a model with data from configurations 1 (pronated forearm) and 4 (supinated forearm) increases the accuracy of the model when used for testing configuration 4. Figure 6-4 shows estimation accuracy of two linear regression models, both used for testing configuration 4: one trained only with configuration 1, and the other trained with both configurations 1 and 4. Both models were trained and tested using data gathered from one of the volunteers.

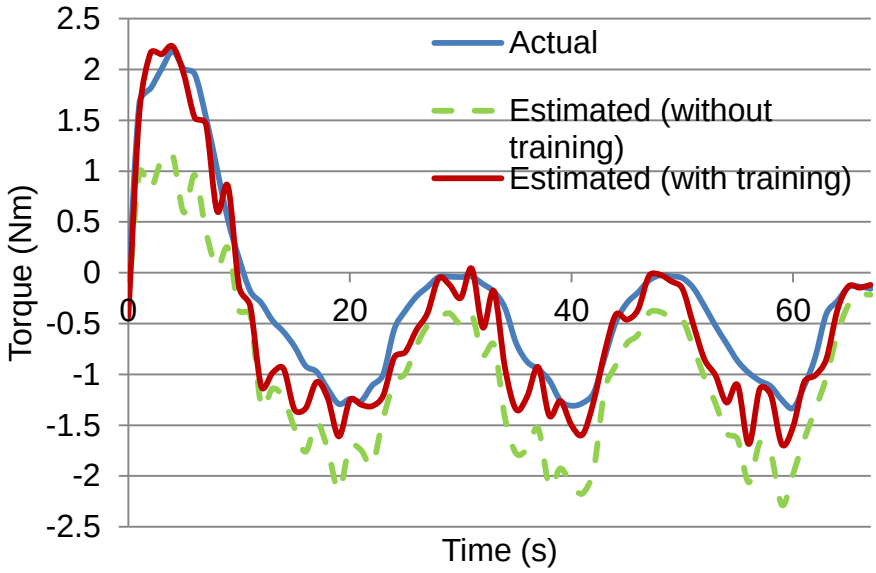

Figure 6-4: Torque estimation with and without explicit forearm supination training.

R^2 value increased by 125%, while NRMSE decreased by 55%. Figure 6-5 visualizes the change in R^2 and NRMSE values in the two scenarios.

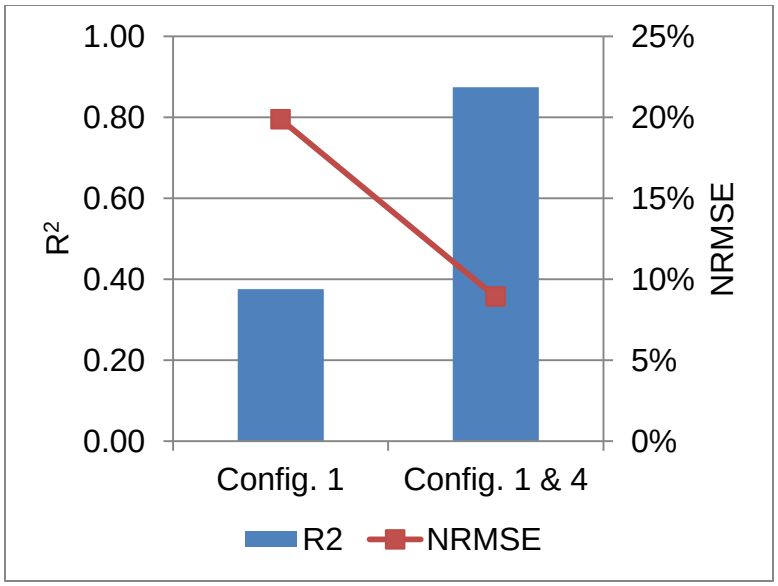

Figure 6-5: Drastic model accuracy increase with explicit forearm supination training.

Results of this experiment demonstrate that model accuracy can be successfully restored with addition of appropriate data to the training data set. Moreover, addition of training data sets at different arm configurations not only increases model accuracy at added configurations but also does not result in a deterioration of previously trained configurations.

Training models with other training sets in addition to configuration 1 did not deteriorate testing accuracy for configuration 1. Figure 6-6 compares estimation mean R^2 and NRMSE of models trained with configuration 1 (group 1), configurations 1 and 2 (group 2), configurations 1 through 3 (group 3), configurations 1 through 4 (group 4), configurations 1 through 5 (group 5), and configurations 1 through 6 (group 6) for testing configuration 1.

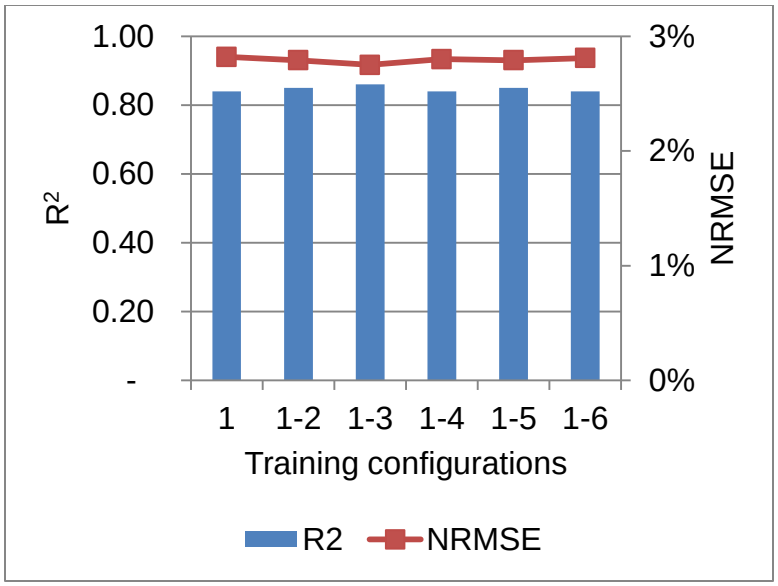

Figure 6-6: Effects of increasing the number of training sets on torque estimation accuracy.

In a more comprehensive experiment, we demonstrated the estimation accuracy of six models trained with groups 1 through 6, for testing data of each of the six configurations. Table 6-3 tabulates the results.

Table 6-3: Mean R^2 for six models trained with groups 1 through 6.

Testing set	Group 1	Group 2	Group 3	Group 4	Group 5	Group 6
1	0.15	0.18	0.16	0.61	0.76	0.83
2	0.17	0.21	0.23	0.64	0.82	0.83
3	0.25	0.24	0.23	0.86	0.83	0.86
4	0.61	0.67	0.84	0.84	0.84	0.82
5	0.58	0.84	0.85	0.83	0.82	0.84
6	0.84	0.83	0.82	0.84	0.86	0.83

Results of this experiment show that with addition of training data, model accuracy is preserved for all configuration that were a part of that training set. For instance, models trained with group 6, that contains all six configurations, had high estimation accuracy for all testing configurations (R^2>0.8). Additionally, for group 4, presence of configuration 4 in the training data set resulted in a boost in estimation accuracy for untrained configurations 5 and 6. Figure 6-7 visualizes estimation accuracy with added training data for all configurations.

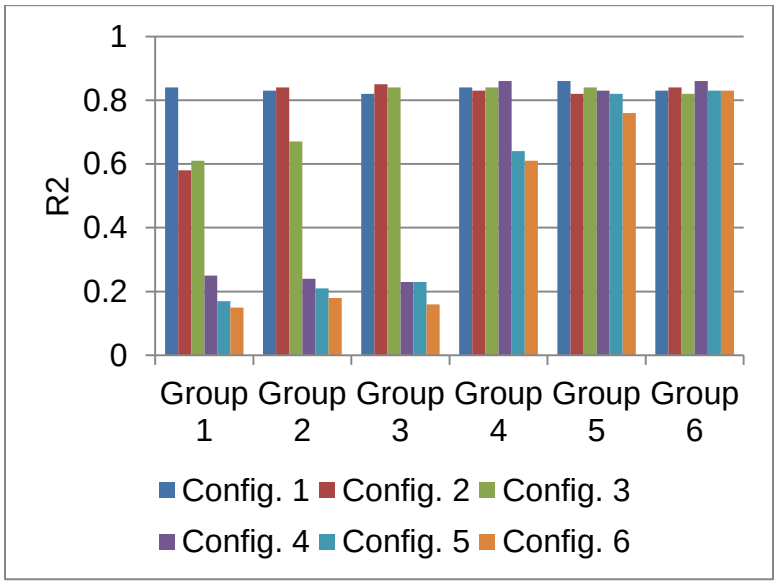

Figure 6-7: Effects of increasing the number of training sets on torque estimation accuracy.

With the addition of training data sets, the regression coefficient vector for the modified linear regression model is updated. With an updated vector, the estimated values for the previously trained data sets are slightly different compared to a model that was not trained with the new data set. For example, with the addition of the training data for configuration 2 (group 2 training), it can

be noticed that the mean R^2 value for configuration 1 is slightly changed compared to the estimation of the model trained with group 1.

The only concern that arises from increasing the size of training data sets is a potential increase in the time it takes for model training. Model training entails computation of coefficients of determination of linear regression model based on training data sets. However, Figure 6-8 illustrates that increasing the number of training sets results in a negligible increase in training times.

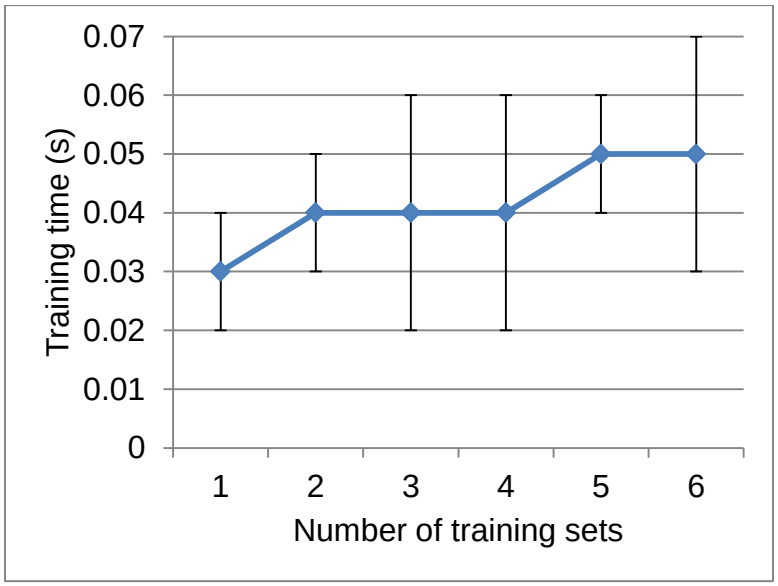

Figure 6-8: Effects of increasing the number of training sets on model training time.

Machine learning regression methods, widely utilized for estimation of joint torques tend to require much longer training times compared to linear regression. For instance, Support Vector Regression requires performance of a procedure called grid search that involves finding the optimal hyperparameters of the model.

This procedure substantially increases training time and is therefore undesirable for explicitly training models at various configurations. Furthermore, for applications with higher required model accuracy, gathering and training models with more training data can further increase model accuracy. Linear regression is an appropriate fit for such applications as the enlarged training data set would not considerably affect training data times.

CHAPTER 7 CONCLUSIONS AND FUTURE WORK

7.1 Conclusions

Eleven healthy volunteers participated in this study. During the first session, 33,520 samples from eight SEMG channels and a torque sensor were acquired while volunteers followed a protocol consisting of isometric flexion and extension of the wrist. We then processed SEMG signals and resampled every 100 samples to save model training time. Subsequently, we trained models using identical training data sets. When using 90% of data as training data set and the rest of the data as testing data, we attained R^2 values of 0.96±0.04, 0.97±0.04, 0.97±0.03, 0.97±0.03, 0.96±3, and 0.87±0.07 for PBM, OLS, RLS, SVM, ANN, and LWPR respectively. All models performed in a very comparable fashion, except for LWPR that yielded lower R^2 values and higher NRMSE values.

Models trained using the data set from session one were tested using two separate data sets gathered one hour and twenty four hours following session one. We showed that Mean R^2 values after one hour decrease 34%, 28%, 25%, 34%, 35%, and 20% for PBM, OLS, RLS, SVM, ANN, and LWPR, respectively. Tests after twenty-four hours showed even further performance deterioration. Therefore, we concluded that all models considered in this study are sensitive to passage of time and electrode displacement.

The effects of the number of SEMG channels used for training were explored. Models trained with SEMG channels from the five primary forearm

muscles were shown to be of similar predictive ability compared to models trained with all eight SEMG channels. However, models trained with two SMEG channels resulted in estimations with lower R^2 and higher NRMSE values.

Finally, models trained with forearm in a pronated position were tested with data gathered from forearm in the supinated position. Mean NRMSE values increased 2.50, 2.10, 2.13, 2.04, 2.24, and 2.32 times for PBM, OLS, RLS, SVM, ANN, and LWPR.

The substantial decrease in predictive ability of all models with passage of time, electrode displacement, and altering arm configurations necessitates regular retraining of models in order to sustain estimation accuracy. We showed that resampling the data set substantially reduces the training time without sacrificing estimation accuracy of models. All models were trained in under 20 seconds while OLS was trained in under 10 ms. Low training times achieved in this work render regular retraining feasible.

We proposed and demonstrated the viability of a modified linear regression for estimation of isometric wrist joint torques with varying arm configurations. We showed that testing accuracy increases with training models with data gathered from different arm configurations. Furthermore, we demonstrated that the model training time does not substantially increase with addition of training data, making the model desirable for training at numerous configurations.

7.2 Future Work

This work was aimed at identifying the best isometric joint torque estimation model available for estimation of wrist joint torques. Only isometric conditions were considered in order to simplify the analysis. However, devices occasionally need to be controlled in dynamic cases where the joint angle is not fixed or changing at a non-constant velocity. Introduction of dynamic motions further increases the complexity of models and models have to be compared under dynamic conditions in the future.

Signal processing, model training, and testing was conducted on a PC equipped with MATLAB software after data acquisition. However, for a portable assistive device, models need to be programmed on a microcontroller and tested in real-time.

The estimation accuracy of the modified linear regression model presented was demonstrated to be robust to varying joint angles with training at different joint angles. Future work will consider training the model under changes of the ulnar/radial deviation degree of freedom for a more comprehensive model as the training time for linear regression model is virtually zero with resampled data.

Human wrist possesses two degrees of freedom. Two independent models can be trained and used for estimation of wrist flexion/extension and ulnar/radial deviation. The resulting system of models can be used to control devices with two degrees of freedom, for instance the WEP device developed at Simon Fraser University [25].

In summary, the following tasks are proposed for developing a comprehensive wrist joint torque estimation model:

- Comparing performance of models under dynamic motions.
- Implementing the OLS model on a microcontroller and testing the performance in real-time.
- Retraining the OLS model with ulnar/radial deviation angle variation data.
- Developing a system consisting of two independent models for estimation of the both wrist flexion/extension and radial/ulnar deviation degrees of freedom.
- Explore the applicability of the models used in this study using SEMG and torque data gathered from the elderly.

APPENDICES

Appendix A: Surface Electromyography (SEMG)

Peak-to-peak amplitude of SEMG signals ranges from 0 to 10mV and its usable energy is in the 0 to 500Hz range with the dominant energy lying in the 50-150Hz range. Therefore, it is essential to sample SEMG signals at a minimum frequency of 1000Hz in order to successfully reconstruct the signal.

Electrical noise complicates the analysis of SEMG signals. Electrical noise has four sources. The first source is the inherent noise in the equipment that cannot be eliminated and can only be attenuated by intelligent circuit design and utilization of high quality electronic components. The second source is ambient noise that can result from the presence of any electromagnetic devices in the environment. Ambient noise amplitudes can be one to three orders of magnitude larger than SEMG signals. The third source is motion artifact that results from either the interface between the surface of the electrodes and the skin or the motion of the connecting cables. The electrical signals of this type have most of their energy in the 0 to 20Hz frequency range. The last source is the inherent instability of the SEMG signals due to their quasi-random nature that is a result of quasi-random nature of the motor units.

Differential electrodes are used to detect SEMG signals. These electrodes can successfully eliminate much of the common signals at the two sites of

attachment (noise signals) so the local SEMG signals can be identified. However, the electronic components that handle subtracting the signals at the two sites are not ideal.

The signal-to-noise ratio of SEMG signals is a function of the chemical reactions between the electrolytes at the surface of the skin and the metal of the surface electrodes. The choice of material at the surface of the electrodes and conductive electrolytes to improve contact with the skin significantly affects the quality of SEMG signals. Moreover, with increasing the distance between the detection surfaces, the amplitude of the SEMG signal increases which is desirable. However, the increased distance increases cross-talk between muscles and also makes SEMG acquisition from smaller muscles impractical.

Special care needs to be taken when attaching electrodes. The longitudinal axis of the electrode should be aligned parallel to the length of the muscle fibers. The longitudinal axis of the electrode is an axis that passes through both detections surfaces. Moreover, the electrodes should not be attached on or near tendons as the number of muscle fibers is decreased and the SEMG signal amplitude diminishes. Despite what was believe over the past half of century, electrodes should not be placed over or near a motor point. These points are the most electrically excitable area of the muscles. Ideally the electrode should be placed between two motor points or a motor point and a tendon.

Appendix B: Support Vector Machines

Epsilon support vector regression (ϵ-SVR), seeks a function f(x) that at most has ϵ deviation from obtained target outputs y_i. This function can be written as followed:

$$f(x) = \langle w, x \rangle + b \tag{B-1}$$

where $\langle w, x \rangle$ is a dot product between w and x.

We must also make sure that f(x) is flat, meaning that the value of w is small. This can be accomplished by minimizing the norm, i.e. $\|w\|^2 = \langle w, w \rangle$. The two conditions can be formulated as a convex optimization problem:

$$\begin{aligned} &\text{minimize} && \frac{1}{2}\|w\|^2 \\ &\text{subject to} && \begin{cases} y_i - \langle w, x_i \rangle - b \leq \epsilon \\ \langle w, x_i \rangle + b - y_i \leq \epsilon \end{cases} \end{aligned} \tag{B-2}$$

However, the above convex optimization problem is not always feasible and we want to allow for some errors. The optimization problem is reformulated to take into account slack variables ξ_i and ξ_i^* that transform the otherwise infeasible optimization problem:

$$\begin{aligned} &\text{minimize} \quad \frac{1}{2}\|w\|^2 + C\sum_{i=1}^{\ell}(\xi_i + \xi_i^*) \\ &\text{subject to} \quad \begin{cases} y_i - \langle w, x_i\rangle - b \le \epsilon + \xi_i \\ \langle w, x_i\rangle + b - y_i \le \epsilon + \xi_i^* \\ \xi_i, \xi_i^* \ge 0 \end{cases} \end{aligned} \tag{B-3}$$

where C is a trade-off parameter between flatness and the amount of variation from ε tolerated, and ℓ is the number of samples.

The optimization problem and its linear constraints can be represented using a Lagrangian function:

$$\begin{aligned} L = \frac{1}{2}|w|^2 + C\sum_{i=1}^{\ell}(\xi_i + \xi_i^*) - \sum_{i=1}^{\ell}\alpha_i(\epsilon + \xi_i - y_i + \langle w.x_i\rangle + b) \\ - \sum_{i=1}^{\ell}\alpha_i^*(\epsilon + \xi_i^* - y_i + \langle w.x_i\rangle - b) - \sum_{i=1}^{\ell}(\eta_i\,\xi_i + \eta_i^*\xi_i^*) \end{aligned} \tag{B-4}$$

Through Lagrangian theory the optimization problem can be transformed into dual form that is a quadratic programming problem with linear conditions and a positive Hessian matrix (ensuring a unique global optimum). Another benefit of this transformation is the possibility of replacing the dot product with a nonlinear transformation on the input vectors. The Gaussian kernel is the most commonly used transformation:

$$k(x, x') = \exp\left(-\frac{\|x - x'\|^2}{2\sigma^2}\right) \tag{B-5}$$

The transformed optimization problem is presented below:

$$\text{maximize} \quad \begin{cases} -\frac{1}{2}\sum_{i,j=1}^{\ell}(\alpha_i - \alpha_i^*)(\alpha_j - \alpha_j^*)k(x_i, x_j) \\ -\epsilon\sum_{i=1}^{\ell}(\alpha_i + \alpha_i^*) + \sum_{i=1}^{\ell} y_i(\alpha_i - \alpha_i^*) \end{cases} \tag{B-6}$$

$$\text{subject to} \quad \begin{cases} \sum_{i=1}^{\ell}(\alpha_i - \alpha_i^*) = 0 \\ \alpha_i, \alpha_i^* \in [0, C] \end{cases}$$

The ε-SVR approximation with Gaussian kernel transformation becomes:

$$f(x) = \sum_{i=1}^{\ell}(\alpha_i - \alpha_i^*)\exp\left(-\frac{\|x - x'\|^2}{2\sigma^2}\right) + b \tag{B-7}$$

Appendix C: Artificial Neural Networks

Neural networks are a set of neurons with adjustable parameters that can be trained to produce a desirable output. The building block of a neural network is a single-input neuron shown in Figure B-1.

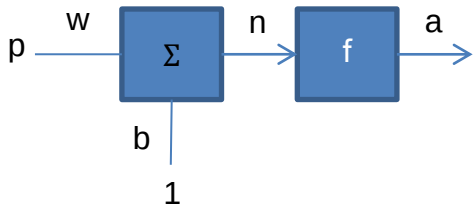

Figure 7-1: Single neuron structure.

The scalar input to the function f is computed by multiplying weight w by scalar input p, and adding bias b to it. Function f subsequently acts on n and produces the output a. Weight w and bias b are adjustable scalar parameters of the neuron.

$$a = f(wp + b) \qquad \text{(C-1)}$$

Different linear and non-linear transfer functions (f) exist that map the input and output. A commonly used transfer function for non-linear mappings is the hyperbolic tangent sigmoid function:

$$\mathbf{a} = \frac{\mathbf{2}}{\mathbf{1} + \exp(-\mathbf{2n})} - \mathbf{1} \qquad \text{(C-2)}$$

A group of neurons can be combined to create a layer. A layer of neurons with an input vector of size R and S neurons, the network will be constructed as shown in Figure B-2.

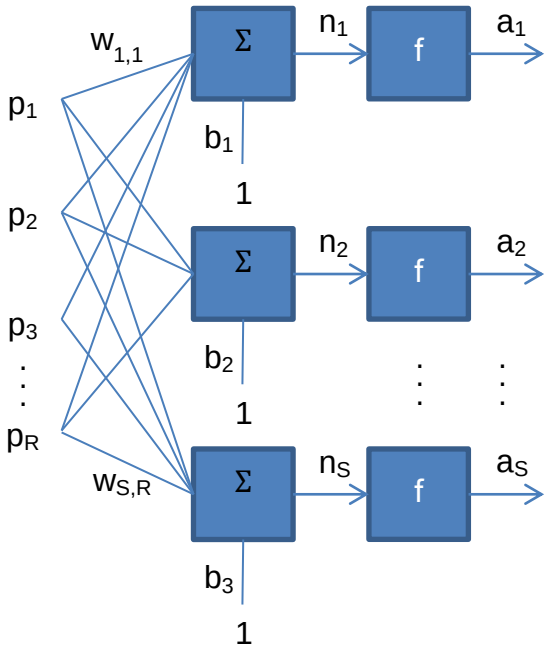

Figure 7-2: One layer of neurons.

In this case the transfer function is acting on a vector rather than a scalar. The output a, is also a vector:

$$\mathbf{a} = \mathbf{f}(\mathbf{Wp} + \mathbf{b}) \tag{C-3}$$

where W is the weight matrix defined as:

$$\mathbf{W} = \begin{bmatrix} \mathbf{w_{1,1}} & \mathbf{w_{1,2}} & \cdots & \mathbf{w_{1,R}} \\ \mathbf{w_{2,1}} & \mathbf{w_{2,2}} & \cdots & \mathbf{w_{2,R}} \\ & & & \\ \mathbf{w_{S,1}} & \mathbf{w_{S,2}} & \cdots & \mathbf{w_{S,R}} \end{bmatrix} \tag{C-4}$$

The same concept can be expanded to networks of multiple layers. In a multiple-layer network, outputs of the first layer are inputs to the second layer and so on. Different transfer functions can be selected at each layer.

Appendix D: Locally Weighted Projection Regression

This appendix intends to illustrate the underlying concept of the Locally Weighted Projection Regression (LWPR) method. Details of implementation and learning methodology are quite extensive and are available in [82].

LWPR approximation method, is at its core a combination of piecewise linear model. Linear models can be used when only a subset of data in the vicinity of a center point for that model is considered:

$$\mathbf{y} = \boldsymbol{\beta}^{\mathbf{T}}\mathbf{x} + \boldsymbol{\epsilon} \tag{D-1}$$

where x is the regressor (input), y is the regressand (output), β is the regression coefficient vector and ε is a vector of random noise values with zero mean.

LWPR automatically determines the number of local models K, regression coefficients for each local model β_K, and region of validity parameterized as distance metric D_k in a Gaussian kernel:

$$\mathbf{w_k} = \mathbf{exp}(-\mathbf{0.5}(\mathbf{x} - \mathbf{c_k})^{\mathbf{T}}\mathbf{D_k}(\mathbf{x} - \mathbf{c_k})) \tag{D-2}$$

where D is a positive distance metric that determines the size and shape of the neighborhood of the local model k and c_k is the center point of local model k.

For every point x, each local linear model provides a estimation denoted as $\hat{y}_k(x)$. Estimated output of the system is the normalized weighted mean of all the K linear models:

$$\hat{\mathbf{y}} = \frac{\sum_{\mathbf{k=1}}^{\mathbf{K}} \mathbf{w_k}\, \hat{\mathbf{y}}_\mathbf{k}}{\sum_{\mathbf{k=1}}^{\mathbf{K}} \mathbf{w_k}} \tag{D-3}$$

Model training is accomplished through an incremental computation of local regression models while adjusting for the distance metric D as more training data are interpreted.

Appendix E: Analysis of Variance (ANOVA)

One-way ANOVA is a method used for comparing the means of two or more data groups. The ANOVA tests the null hypothesis that samples in two or more groups are drawn from the same population with equal mean values. The alternative hypothesis is that at least one of the means is different.

The following assumptions are made about the samples:

- All sample populations are normally distributed.
- All sample populations have equal variance.
- All observations are mutually independent.

However, the ANOVA test is known to be robust to violations of the first two assumptions.

ANOVA measures two sources of variation in the data groups and compares their sizes. The first source of variation is the variation between groups (SSG):

$$\mathbf{SSG} = (\bar{\mathbf{x}}_\mathbf{i} - \bar{\mathbf{x}})^\mathbf{2} \tag{E-1}$$

where $\bar{\mathbf{x}}$ is overall mean (all data groups combined) and $\bar{\mathbf{x}}_\mathbf{i}$ is the mean for the i^{th} data group.

The second source of variation is the variation within groups (SSE):

$$\mathbf{SSE} = \left(\bar{\mathbf{x}}_\mathbf{ij} - \bar{\mathbf{x}}_\mathbf{i}\right)^\mathbf{2} \tag{E-2}$$

where $\bar{\mathbf{x}}_\mathbf{ij}$ is the j^{th} element of the i^{th} data group.

The F-statistic is used for comparison of the components of the variation:

$$\mathbf{F} = \frac{\mathbf{SSG}/(\mathbf{k}-\mathbf{1})}{\mathbf{SSE}/(\boldsymbol{n}-\mathbf{2})} \quad \text{(E-3)}$$

where k is the number of data groups and n is the total number of data in all data groups.

The null hypothesis is rejected if the test statistic from the table is greater than the F critical value with 1 in the numerator and N-2 in the denominator degrees of freedom.

P-value, that is the probability of the null hypothesis to be true, is computed by comparing the F-statistic to the F(k-1,n-k) distribution where k-1 is the numerator and n-k is the denominator of the F distribution. With a P-value of less than 0.05, the mean of at least one of the groups is statistically significant from the other groups.

Appendix F: Noraxon Myosignal 1400L Specifications

The MyoSystem™ 1400L surface and fine-wire electrode SEMG unit is a highly versatile device ideal for research studies. The system is an 8 channel unit. This instrument features Noraxon's internationally patent-protected amplifier technology to provide clean, consistent and reliable SEMG signals during any type of isometric or dynamic exercise. The 1400L has a "built in" USB A/D which handles all data acquisition and greatly simplifies interfacing to a computer for data acquisition.

Features

- Pre-amplified electrode leads, can be used with disposable or permanent electrodes.
- Internal data acquisition system with USB connectivity for 8 channels.
- Compliant with IEC60601-1 and IEC60601-2-40 electromyography standards (CE approved).

Outputs

- Analog +/- 5 volts on all SEMG channels.
- Digital 12 bit resolution per channel from USB port.

Inputs

- 8 SEMG channels @ +/- 7 mV max.
- 8 sensor channels @ +/- 5 Volts max.

- Power 100-240 VAC @ 50/60 Hz (0.9 A max)

SEMG Amplifier Performance

- 1 uV sensitivity.
- < 1 uV RMS baseline noise.

Data Acquisition

- 12 bit resolution 8 channels.
- USB update to PC every millisecond.

High Pass Cutoff

- 10 Hz first order on SEMG channels.

Low Pass Cutoff

- Selectable 500 or 1000 Hz on SEMG channels.
- 8th order Butterworth (maximally flat).

Input Impedance

- > 100 MOhm on SEMG channels (isolated to > 3000 Volts).

Common Mode Rejection

- Min 100 dB @ 50-60 Hz.

Physical

- 11” L x 7.75” W x 4” H; 3 lbs. (28 x 19.7 x 10.2 cm; 1.4 kg).

Appendix G: Transducer Techniques TRT-100 Torque Sensor Specifications

The TRT Series reaction torque sensors offer long term reliability due to non-moving parts and state of the art bonded foil strain gages. Whenever possible, the best approach for precision torque measurements is via reaction torque sensing, eliminating high maintenance and high cost of slip rings, bearings and brushes.

Specifications and dimensions of the torque sensor (Transducer Techniques TRT-100) used in this study are shown in Table D-1 and Figure D-1.

Table 7-1: Torque sensor specifications.

Parameter	Value
Rated output (R. O.)	2mV/V nom
Nonlinearity	0.1% of R. O.
Hysteresis	0.1% of R. O.
Nonrepeatability	0.05% of R. O.
Zero balance	1.0% of R. O.
Compensated temperature range	60° to 160°F
Safe temperature range	-65° to 200°F
Temperature effect on output	0.005% of load/°F
Temperature effect on zero	0.005% of R. O. /°F
Thermal resistance	350Ω nom
Excitation voltage	10 VDC
Safe overload	150% of R. O.
Capacity	100lbs
Torsional stiffness	10, 125 in lbs/rad
Max overhung moment	100 in lbs
Max shear	40 lbs
Max thrust	800 lbs

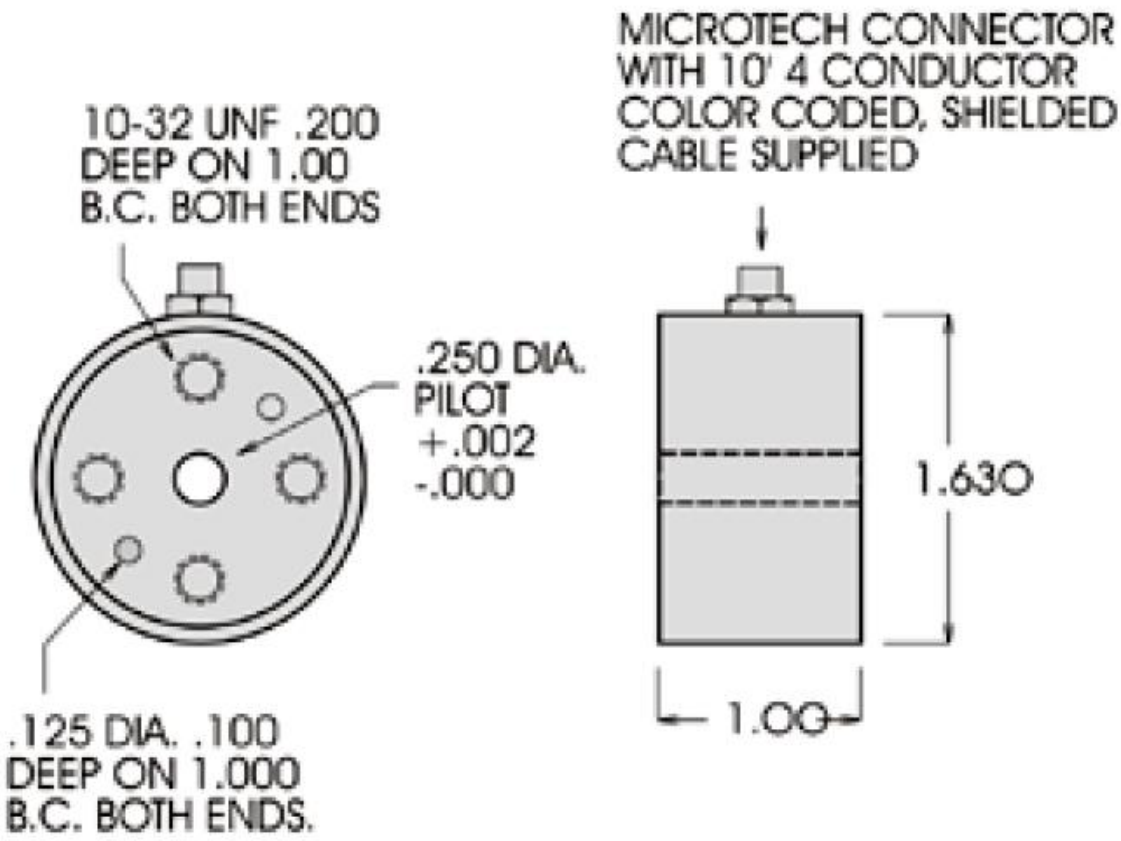

Figure 7-3: Torque sensor dimensions.

REFERENCE LIST

1. Tracking Heart Disease and Stroke in Canada 2009 Public Health Agency of Canada: http://www.phac-aspc.gc.ca/publicat/2009/cvd-avc/index-eng.php.
2. Erol D, Sarkar N: Coordinated Control of Assistive Robotic Devices for Acitivies of Daily Living Tasks. Neural Systems and Rehabilitation Engineering, IEEE Transactions on 2008 16(3):1534-4320.
3. Dellon B, Matsuoka Y: Prosthetics, exoskeletons, and rehabilitation [Grand Challenges of Robotics], Robotics & Automation Magazine, IEEE, 2007 14(1):30-34.
4. Rotella MF, Reuther KE, Hoffman CL, Hage EB, BuSha BF: An orthotic hand-assistive exoskeleton for actuated pinch and grasp. Bioengineering Conference, 2009 IEEE 35th Annual Northeast.
5. Piwko C, Desjardins OB, Bereza BG, Machado M, Jaszewski B, Freedman MS, Einarson TR, Iskedjian M: Pain due to multiple sclerosis: Analysis of the prevalence and economic burden in Canada. Pain Res Manag. 2007 Winter 12(4):259-265.
6. Fu Y, Wang P, Wang S, Liu H, Zhang F: Design and development of a portable exoskeleton based CPM machine for rehabilitation of hand injuries. Robotics and Biomimetics, 2007. ROBIO 2007. IEEE International Conference on.

7. Worsnopp TT, Peshkin MA, Colgate JE, Kamper DG: An Actuated Finger Exoskeleton for Hand Rehabilitation Following Stroke. Rehabilitation Robotics, 2007. ICORR 2007. IEEE 10th International Conference on.
8. Morley JE:The top ten hot topics in aging. Journal of Gerontology: Medical Sciences. 2004 59A(1): 24–33.
9. Doherty JD: Physiology of Aging. Journal of Appl Physiol 2003 95:1717-1726.
10. Kauer JMG: Functional anatomy of the wrist. Clinical Orthopaedics and Related Research, June 1980, Volume 149.
11. Adams BD, Grosland NM, Murphy DM, McCullough M: Impact of impaired wrist motion on hand and upper-extremity performance. Journal of Hand Surgery 2003 28(6)898-903.
12. Koeneman EJ, Schultz RS, Wolf SL, Herring DE, Koeneman JB: A pneumatic muscle hand therapy device. Engineering in Medicine and Biology Society, 2004. IEMBS '04. 26th Annual International Conference of the IEEE.
13. Schaechter JD: Motor rehabilitation and brain plasticity after hemiparetic stroke. Progress in Neurobiology. 73(1):61-72.
14. Krakauer JW: Motor learning: its relevance to stroke recovery and neurorehabilitation. Current opinion in neurology, 2006.
15. Kawasaki H, Ito S, Ishigure Y, Nishimoto Y, Aoki T, Mouri T, Sakaeda H, Abe M: Development of a Hand Motion Assist Robot for Rehabilitation

Therapy by Patient Self-Motion Control. Rehabilitation Robotics, 2007. ICORR 2007. IEEE 10th International Conference on.

16. Gupta A, O'Malley MK: Robotic Exoskeletons for Upper Extremity Rehabilitation. 2007 I-Tech Education and Publishing, Vienna.
17. Shields BL, Main JA, Peterson SW: Strauss AM: An Anthropomorphic Hand Exoskeleton to Prevent Astronaut Hand Fatigue During Extravehicular Activities. 1997 Systems, Man and Cybernetics, Part A: Systems and Humans, IEEE Transactions on. 27(5):668-673.
18. Alvarez B, Iborra A, Alonso A, de la Puente J: Reference architecture for robot teleoperation: development details and practical use. 2001 Control Engineering Practice 9:395-402.
19. Hesse S, Kuhlmann H, Wilk J, Tomelleri C, Kirker GB: A new electromechanical trainer for sensorimotor rehabilitation of paralysed fingers: A case series in chronic and acute stroke patients. Journal of NeuroEngineering and Rehabilitation 2008 5:21.
20. Ueki S, Nishomoto Y, Abe M, Kawasaki H, Ito S, Ishigure Y, Mizumoto J, Ojika T: Development of virtual reality exercise of hand motion assist robot for rehabilitation therapy by patient self-motion control. 30th Annual International IEEE EMBS Conference Vancouver, British Columbia, Canada, August 20-24, 2008.
21. Xing K, Xu Q, He J, Wang Y, Liu Z, Huang X: A wearable device for repetitive hand therapy. Biomedical Robotics and Biomechatronics, 2008.

BioRob 2008. 2nd IEEE RAS & EMBS International Conference on 2008:919-923.

22. Ring H: Controlled study of neuroprosthetic functional electrical stimulation in sub-acute post-stroke rehabilitation. Journal of Rehabilitation Medicine. 2005 37(1):32.
23. Hasegawa Y, Mikami Y, Watanabe K, Sankai Y: Five-fingered assistive hand with mechanical compliance of human finger. Robotics and Automation, 2008. ICRA 2008. IEEE International Conference on 2008:718-724.
24. Takahashi CD, Der-Yeghiain L, Le V, Motiwala RR, Cramer SC: Robot-based hand motor therapy after stroke. Journal of Neurology 131(2):425-437.
25. Henrey M, Sheridan C, Khokhar ZO, Menon C:Towards the development of a wearable rehabilitation device for stroke survivors. Science and Technology for Humanity (TIC-STH), 2009 IEEE Toronto International Conference 26-27.
26. Khokhar et al.: Surface EMG pattern recognition for real-time control of a wrist exoskeleton. BioMedical Engineering OnLine 2010 9:41.
27. A Review of Control Methods for Electric Power Wheelchairs Based on Electromyography Signals with Special Emphasis on Pattern Recognition. IETE Technical Review. 2011. Volume 28, Issue 4.

28. Raez M B I, Hussain M S, Mohd-Yasin F: Techniques of EMG signal analysis: detection, processing, classification and applications. Biol Proced Online 2006, 8:11-35.
29. Mulas M, Folgheraiter M, Gini G: An EMG-controlled Exoskeleton for Hand Rehabilitation. Rehabilitation Robotics, ICORR 2005. 9th International Conference on 2005:371-374.
30. Marchal-Crespo L, Reinkensmeyer DJ: Review of control strategies for robotic movement training after neurologic injury. Journal of NeuroEngineering and Rehabilitation 2009 6:20.
31. Ahsan M R, Ibrahimy M I, Khalifa O O: EMG Signal Classification for Human Computer Interaction: A Review. European Journal of Scientific Research 2009 33(3):480-501.
32. Ferreira A, Celeste WC, Cheein FA, Bastos-Filho TF, Sarcinelli-Filho M, Carelli R: Human-machine interfaces based on EMG and EEG applied to robotic systems. Journal of NeuroEngineering and Rehabilitation 2008 5:10.
33. Kwakkel G, Kollen BJ, Krebs HI: Effects of Robot-Assisted Therapy on Upper Limb Recovery After Stroke: A Systematic Review. Neurorehabilitation and Neural Repair 2007 22:111.
34. Maier-Hein L, Metze, F, Schultz T, Waibel A: Session independent non-audible speech recognition using surface electromyography. Automatic Speech Recognition and Understanding, 2005 IEEE Workshop on 2005:331-336.

35. Zwarts MJ, Drost G, Stegeman DF: Recent progress in the diagnostic use of surface EMG for neurological diseases. Journal of Electromyography and Kinesiology 2000 10:287-291.
36. Cheng EJ, Brown IA, Loeb GE: Virtual muscle: a computational approach to understand the effects of muscle properties on motor control. Journal of Neuroscience Methods 2000 101:117-130.
37. Winter D A, Fuglevand A J, Archer S E: Crosstalk in surface electromyography: Theoretical and practical estimates. Journal of Electromyography and Kinesiology 1994 4(1):15-26.
38. Lateva ZC, Dimitrova NA, Dimitrov GV: Effect of recording electrode position along a muscle fibre on surface potential power spectrum. Journal of Electromyography and Kinesiology 1993 3(4):195-204.
39. Scheme E, Fougner A, Stavdahl Ø, Chan ADC, Englehart K: Examining the adverse effects of limb position on pattern recognition based myoelectric control. Engineering in Medicine and Biology Society (EMBC), 2010 Annual International Conference of the IEEE 2010:6337-6340.
40. De Luca C J: The use of surface electromyography in biomechanics. Journal of Applied Biomechanics 1997 13(2):135-163.
41. Winkel J, Jørgensen K: Significance of skin temperature changes in surface electromyography. Eur J Appl Physiol 1991 63:345-348.
42. Castellini C, van der Smagt P, Sandini G, Hirzinger G: Surface EMG for force control of mechanical hands. Robotics and Automation, 2008. ICRA 2008. IEEE International Conference on 2008:725-730.

43. Hahn ME: Feasibility of estimating isokinetic knee torque using a neural network model. Journal of Biomechanics 2007 40(5):1107-1114.
44. Hughes RE, Chaffin DB: Evaluation of muscle force prediction models of the lumbar trunk using surface electromyography. Journal of Orthopaedic Research 1994 12(5):689-698.
45. Erdemir A, McLean S, Herzog W, van den Bogert AJ: Model-based estimation of muscle forces during movements. Clinical Biomechanics 2007 22:131-154.
46. Cavallaro EE, Rosen J, Perry JC, Burns S: Real-time Myoprocessors for a Neural Controlled Powered Exoskeleton Arm. IEEE Transactions on Biomedical Engineering 2006 53(11):2387-2396.
47. Zhao J, Xie Z, Jiang L, Cai H, Hirzinger G: Levenberg-Marquardt Based Neural Network Control for a Five-fingered Prosthetic Hand. Robotics and Automation, 2005. ICRA 2005. Proceedings of the 2005 IEEE International Conference on 2005:4482-4487.
48. Castellini C, van der Smagt P: Surface EMG in advanced hand prosthetics. Biol Cybern 2009 100:35-47.
49. Park W, Kwon S, Kim J: Real-Time Estimation of Thumb-Tip Forces using Surface Electromyogram for a Novel Human-Machine Interface. IEEE International Conference on Robotics and Automation 2010:205-210.
50. Rosen J, Fuchs M B, Arcan M: Performance of Hill-Type and Neural Network Muscle Models – Towards a Myosignal-Based Exoskeleton. Computers and Biomedical Research 1999 32:415-439.

51. Yang D, Zhao J, Gu Y, Jiang L, Liu H: EMG Pattern Recognition and Grasping Force Estimation: Improvement to the Myocontrol of Multi-DOF Prosthetic Hands. IEEE/RSJ International Conference on Intelligent Robots and Systems 2009.
52. Liu MM, Herzog W, Savelberg HH: Dynamic muscle force predictions from SEMG: an artificial neural network approach. Journal of Electromyography and Kinsiology. Volume 9, Issue 6, December 1999, Pages 391-400.
53. Lloyd D G, Besier T F: An EMG-driven musculoskeletal model to estimate forces and knee joint moment in vivo. Journal of Biomechanics 2003 36:765–776.
54. Carmeli E, Patish H, Coleman R: The aging hand Journal of Gerontology: Medical Sciences 2003 58A(2):146–152.
55. Guimarães, AC, Herzog W, Allinger TL, Zhang YT: The EMG–force relationship of the cat soleus muscle and its association with contractile conditions during locomotion. Journal of Experimental Biology 1995 198:975–987.
56. Van Ruijven LJ, Weijs WA: A new model for calculating muscle forces from electromyograms. European Journal of Applied Physiology and Occupational Physiology 1990 61:479–485.
57. Milner-Brown HS, Stein RB, Yemm R: Changes in firing rate of human motor units during linearly changing voluntary contractions. J Physiol. 1973 230(2):371-90.

58. Rabiner LR, Gold B: Theory and application of digital signal processing. 1975 Prentice Hall.
59. Corcos DM, Gottlieb GL, Latash ML, Almeida GL, Agarwal GC: Electromechanical delay: An experimental artifact. Journal of Electromyography and Kinesiology 1992 2:59–68.
60. Woods JJ, Bigland-Ritchie B: Linear and non-linear surface EMG/force relationships in human muscles. An anatomical/functional argument for the existence of both. American Journal of Physical Medicine. 1983 62:287–299.
61. Manal K, Buchanan TS: Modeling the non-linear relationship between EMG and muscle activation. Journal of biomechanics. 2003 36:1197-1202.
62. Perry J, Bekey GA: EMG-force relationship in skeletal muscle. 1981 Critical review in biomedical engineering.
63. Jacobson MD, Raab R, Fazeli BM, Abrams RA, Botte MJ, Lieber RL: Architectural design of the human intrinsic hand muscles. J. Hand Surg. 1992 17A:804-809.
64. Lieber RL, Jacobson MD, Fazeli BM, Abrams RA, Botte MJ: Architecture of selected muscles of the arm and forearm: anatomy and implications for tendon transfer. J. Hand Surg. 1992 17A:787-798.
65. Lieber RL, Fazeli BM, Botte MJ: Architecture of selected wrist flexor and extensor muscles. J. Hand Surg. 15A:244-250.

66. Brand A R, Douglas R P, Friederich J A: The sensitivity of muscle force predictions to changes in physiologic cross-sectional area. Journal of Biomechanics 19:589-596.
67. Lew HL, TSAI SJ: Pictorial guide to muscles and surface anatomy. In Johnson's practical electromyography. Edited by: Pease WS, Lew HL, Johnson EW. Lippincott Williams and Wilkins; 4 2007:145-212.
68. Gonzalez RV, Buchanan TS, Delp SL: How muscle architecture and moment arms affect wrist flexion-extension movements. J. Biomechanics 1997 30(7):705-712.
69. Yamaguchi GT, Sawa AGU, Moran DW, Fessler MJ, Winters JM: Appendix: a survey of human musculotendon actuator parameters. In: Winters JM, Woo SL-Y editors. Multiple Muscle Systems: Biomechanics and Movement Organization. Springer, New York, 1990 717–773.
70. Brand PW, Hollister AM: Clinical Mechanics of the Hand. Mosby 1999.
71. Buchanan T S, Lloyd D G, Manal K, Besier: Neuromusculoskeletal Modeling: Estimation of Muscle Forces and Joint Moments and Movements From Measurements of Neural Command. J Appl Biomech 2004 20(4):367-395.
72. Whitley D: A genetic algorithm tutorial. Stat. Comp 1994.4(2):65–85.
73. Global Optimization Toolbox User's Guide Mathworks.
74. Chatterjee S, Hadi S A: Influential Observations, High Leverage Points, and Outliers in Linear Regression. Statistical Science 1998 1(3):379-416.

75. Tibshirani R: Regression shrinkage and selection via the Lasso. Journal of Royal Statistical Society. Series B (Methodological) 1996 58(1):267-288.
76. Kim SJ, Koh K, Lustig M, Boyd S, Gorinevsky D: An Interior-Point Method for Large-Scale ℓ1-Regularized Least Squares. IEEE Journal of Selected Topics in Signal Processing 2007 1(4):606-617.
77. Mei Xue, Ling H, Jacobs DW: Sparse Representation of Cast Shadows via ℓ_1-Regularized Least Squares. Computer Vision, 2009 IEEE 12th International Conference on. 583-590.
78. Koh K, Kim SJ, Boyd S: l1_ls: A MATLAB Solver for Large-Scale ℓ1-Regularized Least Squares Problems software available at http://www.stanford.edu/~boyd/l1_ls/
79. Bishop C M: Pattern recognition and machine learning, Springer 2006 325-358.
80. Chang CC, Lin CJ: LIBSVM: a library for support vector machines. 2001 Software available at http://www.csie.ntu.edu.tw/~cjlin/libsvm
81. Smola A J, Schölkopf B: A tutorial on support vector regression. Statistics and Computing 2004 14:199-222.
82. Wang W, Xu Z, Lu W, Zhang X: Determination of the spread parameter in the Guassian kernel for classification and regression. Neurocomputing 2003 55:643-663.
83. Wang L, Buchanan T S: Prediction of Joint Moments Using a Neural Network Model of Muscle Activations from EMG Signal. IEEE

Transactions on Neural Systems and Rehabilitation Engineering. 10(1):30-37.

84. Hiraiwa A, Shimohara K, Tokunaga Y: EMG Pattern Analysis and Classification by Neural Network. Systems, Man and Cybernetics, 1989. Conference Proceedings, IEEE International Conference on 1989 3:1113-1115.
85. Khanna T: Foundations of neural networks Addison-Wesley, Reading, MA 1990.
86. Rumelhart D E, Hinton G E, Williams R J: Learning representations by back propagation errors. .Nature 1986 323:533-536.
87. Setiono R, Hui L C K: Use of a quasi-Newton method in a feedforward neural network construction algorithm. IEEE Trans Neural Netw. 1995 6(1):273-7.
88. Beale M H, Hagan M T, Demuth H B: Neural Network Toolbox 7 User's Guide.
89. Vijayakumar S, D'Souza A, Schaal S: Incremental Online Learning in High Dimensions. Neural Comput 2005 17:2602-2634.
90. Klanke S: software available at http://mloss.org/software/view/65/
91. Shenoy P, Miller KJ, Crawford B, Rao RPN: Online Electromyographic Control of a Robotic Prosthesis, IEEE Transactions on Biomedical Engineering, Vol. 55, No. 3.

92. Delp S L, Grierson A E, Buchanan T S: Maximum isometric moments generated by the wrist muscles in flexion-extension and radial-ulnar deviation. Journal of Biomechanics 1996 29(1):1371-1375.
93. SENIAM Project. Available online at http://www.seniam.org.
94. Draper N R, Smith H: Applied Regression Analysis. Wiley 1998.
95. Koike Y, Kawato M: Estimation of dynamic joint torques and trajectory formation from surface electromyography signals using a neural network model. Biol. Cybern. 1995 73:291-300.
96. Fukuda O, Tsuji T, Kaneko M, Otsuka A: A Human-Assisting Manipulator Teleoperated by EMG Signals and Arm Motion. IEEE Transactions on Robotics and Automation 2003 19(2):210-222.